Macroscopic Coupled Traffic and Energy Model in Front-tracking and Cell-based Frameworks

Mladen Čičić, Carlos Canudas de Wit

Macroscopic Coupled Traffic and Energy Model in Front-tracking and Cell-based Frameworks

Mladen Čičić and Carlos Canudas-de-Wit

Abstract

As the transportation and power systems grow ever more coupled, through the introduction of electric vehicles and their connection with electricity markets, modelling the traffic and energy flows in a joint manner is becoming increasingly important. To this end, we propose a generalized Coupled Traffic and Energy Model, which is able to model the dynamics of electric vehicle state of charge, coupled with the dynamics of the traffic flow. We define and solve a Riemann-like problem for this model, which enables the formulation of numerical schemes for finding the overall solution. Based on the application of front-tracking on the model, which in the studied case provides exact solutions, we propose an extension to the Front-tracking Transition System Model, extending it to include advected energy and ramp flows. This model is used to provide exact solutions, enabling us to define two approximate cell-based models, which are significantly simpler to implement. The proposed models are then tested and compared in an illustrative simulation example. The simulations show that the proposed Front-tracking Transition System Model with advected Energy is able to reproduce diverse traffic scenarios with no loss of information, and that the cell-based models provide a good approximation, simplifying the computations and implementation with little loss of details.

I. Introduction

The accelerating pace of electrification of road transport promises to contribute immensely towards the push for decarbonization of all economic sectors. With the share of battery electric vehicles (EVs) projected to reach 40% in the EU by 2030 [1], it is clear that this development will significantly reduce the transportation emissions. In addition to the transportation sector, the massive arrival of EVs will have a large effect on the power sector, on one hand straining it due to their charging power demands [2], [3], and on the other hand helping it by providing untapped energy storage capabilities, which will be crucial in integrating a higher portion of renewable energy sources and reducing curtailment [4]. Given these developments, it is highly likely that the coupling between the traffic and the power networks is going to significantly increase in the near future. Therefore, a unified modelling framework, able to capture the dynamics of EV traffic, battery dynamics, charging, and the broader power system, will be instrumental in efficiently managing the decarbonization of both the transportation and the power sector.

A large portion of works from the power systems side has focused on coordinating EV charging and discharging, including vehicle-to-grid (V2G), where EV batteries can be used to provide ancillary services [5], [6]. Some works look at the coupled transportation-power system [7], [8], approaching the problem at network scale and using traffic assignment to model the movement of EVs. However, since the focus of these works is on the power system side, they do not provide a detailed description of EV dynamics outside of the charging stations. On the other side, there has recently been a lot of work done on modelling individual EVs, including their battery dynamics. In [9], the power consumption (as well as recovery, through regenerative braking) of EVs was modelled based on its propulsion and braking forces. Other factors, such as driving behaviour and other ambient influences, are considered in [10]. These and similar power consumption models, together with data-driven approaches including real-time traffic data [11] and microscopic simulations [12], have been used to forecast the EV battery state evolution.

However, there is a literature gap on the macroscopic traffic modelling including EVs, describing coupled flows of EVs and energy carried in their batteries. In [13] the authors used a second-order macroscopic traffic model to generate power demand for charging, but only incorporate the information about the EV State of Charge (SoC) through splitting the vehicles into discrete classes. In [14], a macroscopic electromobility model was proposed, coupling the EV traffic with their battery dynamics, both while driving on the road, and while at a charging station. To the authors' best knowledge, these two works are the only ones so far that tackle the EV traffic and energy flows from the macroscopic modelling perspective. In this work, we intend to extend and generalize the results of [14], in both the theoretical and the practical aspects.

First order traffic models have been studied in detail, and many efficient methods for finding their solutions in many different situations have been proposed [15], [16]. Two of the most widely used numerical schemes for solving general partial differential equations, Godunov scheme [17] and front-tracking [18], have been applied to the LWR model. The application of the former results in the well-known Cell Transmission Model [19], whereas the second one has recently been used as a basis for the Front-tracking Transition System Model (FTSM) [20]. Both of these schemes rely on solutions to Riemann problems at discontinuities, whether in the traffic density (at the interface between cells or at fronts) or the flux function [21]. Discontinuities may also arise if additional constraints are imposed on the traffic density or flow due to e.g., moving bottlenecks [22], or if there are on- or off-ramps [23].

Mladen Čičić and Carlos Canudas-de-Wit are with Univ. Grenoble Alpes, CNRS, Inria, Grenoble INP, GIPSA-lab, 38000 Grenoble, France (e-mail: {cicic.mladen, carlos.canudas-de-wit}@gipsa-lab.fr)

The GSOM (Generic second order modelling) [24] family of traffic models has seen active research lately. Apart from the traffic density, these models include an additional advected property which may affect the traffic flow. Whereas the traffic density dynamics are described by the well-known Lighthill-Whitham-Richards (LWR) model [25], [26], the dynamics and nature of the additional property differ throughout the models of this family. A prominent example of these models is the Aw-Rascle-Zhang (ARZ) model [27], [28], where the advected property is the traffic "pressure". One particularly interesting choice for the case studied here is to consider the SoC of EV traffic as the advected property, yielding the model proposed in [14]. However, applying the two mentioned numerical schemes is much harder in the case of GSOM than in the case first-order models. While it is possible to define Riemann solvers, Godunov schemes [29], and front-tracking [30] in some specific cases, a general formulation, which would include all the additional elements required for modelling real-world road traffic, remains difficult to devise. For the case of electromobility, which is studied here, the most relevant additional elements are flux and battery discharge functions defined piecewise in space, and on- and off-ramp flows.

The main contribution of this work is in proposing and analysing a more general version of the Coupled Traffic and Energy Model, first proposed in [14], allowing for generic continuous piecewise-linear flux functions, defining flux and battery discharge functions piecewise in space, and introducing on- and off-ramp flows. We define and solve a generalization of the Riemann problem, with ramp flows and possibly piecewise defined flux and battery discharge functions, and where the initial SoC data is piecewise-linear instead of piecewise-constant as is standard. We then show that this Riemann-like problem solution is of the same form as the initial data, with piecewise-constant traffic density and piecewise-linear SoC, and use this fact to extend the FTSM [20] to include advected SoC and ramp flows. The extended model yields exact solutions in case all flux functions are continuous and piecewise-linear, and we use it as the ground truth to develop and compare in simulations two cell-based models, one based on the Godunov scheme, and one in which the SoC dynamics are simplified.

The rest of this paper is organized as follows. In Section II, we introduce the proposed coupled traffic and energy model, and then in Section III discuss and solve the Riemann-like problem, which will be a key element of the proposed models. Next, in Section IV, we discuss front-tracking solutions to the coupled traffic and energy model, and reformulate it in the FTSM framework. The resulting extended model is then use to propose two cell-based discretizations in Section V, which are then tested in simulations and compared to the exact solution in Section VI. Finally, in Section VII, we summarize the results and outline some future work directions.

II. Coupled traffic and energy model

In this section, we derive and present the Coupled Traffic and Energy (CTE) model that captures the evolution of traffic density, a conserved quantity, as well as an additional nonconserved quantity, which is advected by the vehicles in the traffic flow and dissipated over time. In particular, the nonconserved quantity we study is the SoC of electric vehicles in traffic. We first present the model of the traffic flow, and then augment it with the model of the SoC dynamics, which we assume to not affect the traffic dynamics.

A. Traffic model

We model the dynamics of the traffic flow using the well-known LWR model [25], [26],

$$\frac{\partial \rho}{\partial t} + \frac{\partial q}{\partial x} = 0, \tag{1}$$

omitting arguments for readability, where $\rho(x,t)$ denotes the traffic density at position x and time t, and $q(x,t)$ is the traffic flow, given as a function of the traffic density,

$$q(x,t) = Q(\rho(x,t)), \tag{2}$$

where $Q(\rho)$ is the flux function (also known as fundamental diagram) that describes this dependence. The speed of a vehicle inside of the traffic flow at position x and time t is denoted $v(x,t)$, and given by

$$v(x,t) = \frac{q(x,t)}{\rho(x,t)}, \tag{3}$$

which depends only on traffic density $\rho(x,t)$, since the traffic flow is also a function of it. We also write $v(x,t) = \mathcal{V}(\rho(x,t))$, with $\mathcal{V}(\rho)$ defined by $Q(\rho) = \mathcal{V}(\rho)\rho$.

We may use the traffic density space-time profile $\rho(x,t)$ to reconstruct the trajectories of individual vehicles in the traffic flow. Denote by $x_\xi(t)$ the trajectory of vehicle ξ, starting from some initial position at $t = 0$, $x_\xi(0) = x_\xi^0$. The trajectory of vehicle ξ then evolves according to

$$\dot{x}_\xi(t) = v_\xi(t) = v(x_\xi(t), t), \tag{4}$$

and the vehicle moves at speed defined by the traffic density at its position. Due to the fact that the vehicle trajectories in the LWR model do not intersect, each point in space and time (x,t) uniquely corresponds to the trajectory of a single vehicle $\xi(x,t)$, for which $x_\xi(t) = x$.

B. Energy model

The discharge rate of EV batteries depends on a plethora of influences [10], but the main contributor is naturally their motion. We denote the SoC of vehicle ξ as $\varepsilon_\xi(t) \in [0,1]$, and approximate its discharge during driving as

$$\dot{\varepsilon}_\xi(t) = \mathcal{D}_\xi(v_\xi(t)), \tag{5}$$

where $\mathcal{D}_\xi(v)$ models the battery discharge as a function of the vehicle speed. Assuming all vehicles ξ are electric, we may instead define the macroscopic SoC of all vehicles at different positions on the road $\varepsilon(x,t) \in [0,1]$,

$$\varepsilon(x_\xi(t),t) = \varepsilon_\xi(t). \tag{6}$$

If additionally all vehicles have the same battery discharge dynamics,

$$\mathcal{D}(v(x_\xi(t),t)) = \mathcal{D}_\xi(v_\xi(t)), \tag{7}$$

and always have a high enough SoC so that it does not affect their operation (i.e., so that they do not run low on battery), we may describe the macroscopic evolution of $\varepsilon(x,t)$ by substituting (7) and (6) into (5), yielding

$$\frac{\mathrm{d}\varepsilon(x_\xi(t),t)}{\mathrm{d}t} = \frac{\partial\varepsilon(x,t)}{\partial x}(x_\xi(t),t)\dot{x}_\xi(t) + \frac{\partial\varepsilon(x,t)}{\partial t}(x_\xi(t),t) = \mathcal{D}(v(x_\xi(t),t)),$$

which holds for all vehicles ξ, and consequently, for all $x = x_{\xi(x,t)}(t)$. Finally, substituting (4), and replacing $x_\xi(t)$ by x, we recover the macroscopic SoC model,

$$\frac{\partial\varepsilon}{\partial t} + v\frac{\partial\varepsilon}{\partial x} = d, \tag{8}$$

with the traffic speed $v(x,t)$ given by (3), and the macroscopic battery discharge rate $d(x,t)$ defined as

$$d(x,t) = \mathcal{D}(v(x,t)). \tag{9}$$

This model is an inhomogeneous linear transport PDE with speed varying in space and time as a function of traffic density. Using the method of characteristics on (8), we may confirm that the SoC along trajectories of the vehicles given by (4) evolves as (5), as was the initial assumption.

Equivalently, (8) can be written in terms of normalized energy density $\rho\varepsilon$ as

$$\frac{\partial\rho\varepsilon}{\partial t} + \frac{\partial(v\rho\varepsilon)}{\partial x} = \rho d, \tag{10}$$

which can be verified by expanding the left side of the equation, yielding

$$\left(\frac{\partial\rho}{\partial t} + \frac{\partial q}{\partial x}\right)\varepsilon + \rho\left(\frac{\partial\varepsilon}{\partial t} + v\frac{\partial\varepsilon}{\partial x}\right) = \rho d,$$

and then substituting (1) and (8). In this case, the flow of normalized energy is given by $v\rho\varepsilon$, and the dissipation of energy by the inhomogeneous part ρd. Note that the energy density is normalized by the average battery capacity of the vehicles. This may even include the internal combustion engine vehicles, counting their battery capacity as zero.

The battery discharge function $\mathcal{D}(v)$ can take an arbitrary form, and many different battery models have been proposed [9]–[12]. For simplicity, we will assume $\mathcal{D}(v)$ is a polynomial function, with the constant term capturing the auxiliary power consumption (e.g. for heating or air conditioning), the first order term mostly reflecting the change in potential energy due to vertical displacement (climbing or descending) dominantly affected by road grade, and higher order terms capturing the effects of resistive forces. The simplest way to model battery discharge rate is by assuming it is linearly proportional to vehicle speed, yielding $\mathcal{D}_\xi(x_\xi(t)) = D_1\dot{x}_\xi(t)$ and $\mathcal{D}(v) = D_1 v$, $D_1 < 0$, in which case the spent energy depends only on the distance travelled,

$$\varepsilon_\xi(t_2) - \varepsilon_\xi(t_1) = \int_{t_1}^{t_2} \mathcal{D}(v_\xi(t))\mathrm{d}t = D_1(x_\xi(t_2) - x_\xi(t_1))$$

if $v_\xi(t) \geq 0$ for all t, and the range of the EV is $-\frac{1}{D_1}$.

A special form of the problem is for $\mathcal{D}(v) = 0$, in which case we model the advection of some quantity ε by vehicles in traffic, and the model belongs to the GSOM family [24]. One particularly useful advected quantity is the macroscopic total electric vehicle battery capacity $\bar{\varepsilon}(x,t)$, whose dynamics can be described by (8) or (10), with $\bar{\varepsilon}$ instead of ε, and the inhomogeneous part set to zero, $d = 0$. This gives us an easy way to recover the total energy density on the road, as $\rho\varepsilon\bar{\varepsilon}$.

III. Riemann-like problem

The solution to Riemann problem, which is an initial value problem of a conservation law to piecewise-constant initial conditions with a single discontinuity, is an important component in deriving many numeric schemes for finding conservation law solutions (e.g. Godunov scheme, front-tracking). In this section, we study a generalization of the Riemann problem for the CTE model (1), (8), allowing a more general form of initial conditions $\varepsilon(x,0)$.

In particular, we are interested in the case when the flux function $Q(\rho)$ is continuous and piecewise linear of the form

$$Q(\rho) = \begin{cases} V_1\rho, & 0 \le \rho \le \sigma_1, \\ Q(\sigma_1) + V_2(\rho - \sigma_1), & \sigma_1 < \rho \le \sigma_2, \\ \vdots & \\ Q(\sigma_{i-1}) + V_i(\rho - \sigma_{i-1}), & \sigma_{i-1} < \rho \le \sigma_i, \\ \vdots & \\ Q(\sigma_{m_j}) + V_m(\rho - \sigma_m), & \sigma_m < \rho \le \sigma_{m+1}, \\ 0, & \rho > \sigma_{m+1}, \end{cases} \tag{11}$$

with $Q(\sigma_m) + V_m(\sigma_{m+1} - \sigma_m) = 0$, where V_i denote the slopes of the function and σ_i its breakpoints, and assume that

$$(\forall j < i) \quad \sigma_i Q(\sigma_j) > \sigma_j Q(\sigma_i), \tag{12}$$

i.e., that the traffic speed $\mathcal{V}(\rho)$ is monotonically nonincreasing with ρ. This assumption holds trivially for the majority of used flux functions, since they are typically taken to be concave, but also holds for some non-concave flux functions. Flux functions of this form can represent all most commonly used fundamental diagrams, either exactly, as in the case of e.g. the triangular fundamental diagram, or approximately, as in the case of smooth fundamental diagrams such as Greenshields', with an arbitrarily close fit as the number of breakpoints of Q increases.

A. *Basic case*

We study the initial value problem of (1) and (8), with $q(x,t)$ given by (2), $v(x,t)$ by (3), $d(x,t)$ by (9), flux function (11), and initial conditions

$$\rho(x,0) = \begin{cases} \rho_-, & x < 0, \\ \rho_+, & x > 0, \end{cases} \tag{13}$$

$$\varepsilon(x,0) = \begin{cases} \varepsilon_- + \chi_- x, & x < 0, \\ \varepsilon_+ + \chi_+ x, & x > 0, \end{cases} \tag{14}$$

Note that, contrary to standard practice for Riemann problems, we allow $\varepsilon(x,0)$ to take a more general piecewise-linear form with a single discontinuity at $x = 0$, defined by its left and right limits ε_- and ε_+, respectively, the SoC gradient upstream of the discontinuity χ_-, and the SoC gradient downstream of the discontinuity χ_+. The initial traffic density is defined by the constant traffic density upstream (ρ_-) and downstream (ρ_+) of the discontinuity, as is standard for the Riemann problem. The solution to this Riemann-like problem for $t \ge 0$ is of the form

$$\rho(x,t) = \begin{cases} \rho_1, & x < \lambda_1 t, \\ \rho_2, & \lambda_1 t < x < \lambda_2 t, \\ \quad \vdots & \\ \rho_n, & \lambda_{n-1} t < x < \lambda_n t, \\ \rho_{n+1}, & x > \lambda_n t, \end{cases} \qquad \varepsilon(x,t) = \begin{cases} \varepsilon_1 + \theta_1 t + \chi_1 x, & x < \lambda_1 t, \\ \varepsilon_2 + \theta_2 t + \chi_2(x - \lambda_1 t), & \lambda_1 t < x < \lambda_2 t, \\ & \vdots \\ \varepsilon_n + \theta_n t + \chi_n(x - \lambda_{n-1} t), & \lambda_{n-1} t < x < \lambda_n t, \\ \varepsilon_{n+1} + \theta_{n+1} t + \chi_{n+1}(x - \lambda_n t), & \lambda_n t < x < \lambda_{n+1} t, \\ \varepsilon_{n+2} + \theta_{n+2} t + \chi_{n+2}(x - \lambda_{n+1} t), & x > \lambda_{n+1} t. \end{cases} \tag{15}$$

An example solution to the Riemann-like problem is given in Fig. 1. In this case, the flux function, shown in Fig. 1a, is a piecewise-linear approximation of the Greenshields fundamental diagram, and the traffic density solution is a rarefaction fan from ρ_- to ρ_+. Note that for the initial value of SoC, we have $\chi_- < 0$ and $\chi_+ > 0$.

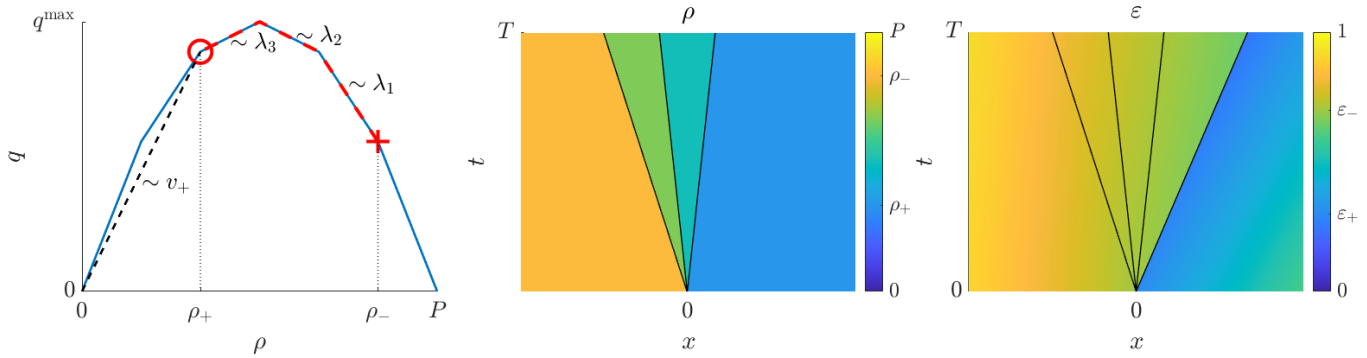

(a) Flux function $q = Q(\rho)$ (b) Traffic density solution $\rho(x,t)$ (c) SoC solution $\varepsilon(x,t)$

Fig. 1: Example solution of the Riemann-like problem.

First, due to the fact that the dynamics of $\rho(x,t)$ do not depend on $\varepsilon(x,t)$, the traffic density part of the solution is given as the solution to the Riemann problem for (1), with $q(x,t)$ given by (2) and initial conditions (13), which is discussed in more detail in [20]. The resulting traffic density $\rho(x,t)$ is piecewise-constant in space and time, and has n fronts propagating at speed λ_i. Here we define fronts as the boundary of the intervals that piecewise define $\rho(x,t)$ or $\varepsilon(x,t)$, e.g., $x=\lambda_i, i=1,\dots,n+1$ in case of (15). The parameters of $\rho(x,t)$, ρ_i, $i=1,\dots,n+1$ and λ_i, $i=1,\dots,n$ are given by

$$\rho_i=\begin{cases}\tilde{\sigma}_{i-1}, & \rho_-<\rho_+,\\ \tilde{\sigma}_{n+1-i}, & \rho_->\rho_+,\end{cases}\quad \lambda_i=\begin{cases}\tilde{V}_{i-1}, & \rho_-<\rho_+,\\ \tilde{V}_{n-i}, & \rho_->\rho_+,\end{cases}$$

where $\tilde{\sigma}_i$ and $\tilde{V}_i$ are the parameters of function $\tilde{Q}(\rho)$,

$$\tilde{Q}(\rho)=\begin{cases}Q(\tilde{\sigma}_0)+\tilde{V}_0(\rho-\tilde{\sigma}_0), & \tilde{\sigma}_0\le\rho<\tilde{\sigma}_1,\\ Q(\tilde{\sigma}_1)+\tilde{V}_1(\rho-\tilde{\sigma}_1), & \tilde{\sigma}_1\le\rho<\tilde{\sigma}_2,\\ \qquad\vdots & \\ Q(\tilde{\sigma}_{n-1})+\tilde{V}_{n-1}(\rho-\tilde{\sigma}_{n-1}), & \tilde{\sigma}_{n-1}\le\rho<\tilde{\sigma}_n,\end{cases}$$

defined on $[\tilde{\sigma}_0,\tilde{\sigma}_n]$, where $\tilde{\sigma}_0=\min\{\rho_-,\rho_+\}$, and $\tilde{\sigma}_n=\max\{\rho_-,\rho_+\}$, as the upper concave envelope of $Q(\rho)$ if $\rho_->\rho_+$, or the lower convex envelope of $Q(\rho)$ if $\rho_-<\rho_+$, on the same interval $[\tilde{\sigma}_0,\tilde{\sigma}_n]$. It is straightforward to verify that $\rho_1=\rho_-$ and $\rho_{n+1}=\rho_+$. Furthermore, we define the column vector ${}^{\rho_-}\tilde{\Sigma}_Q^{\rho_+}=[\rho_1,\dots,\rho_{n+1}]^\top$ of traffic densities present in the solution to the Riemann problem given ρ_-, ρ_+, and Q, and write the length of this vector ${}^{\rho_-}\tilde{m}_Q^{\rho_+}=n+1$. The resulting ρ_i and λ_i satisfy the Rankine-Hugoniot condition,

$$Q(\rho_{i+1})-Q(\rho_i)=\lambda_i(\rho_{i+1}-\rho_i),\quad i=1,\dots,n, \tag{16}$$

i.e., the front propagation speeds λ_i are equal to the slopes of the envelope $\tilde{Q}(\rho)$. In the example presented in Fig. 1, $\tilde{Q}(\rho)$ corresponds to the upper concave envelope of $Q(\rho)$ from ρ_+ to ρ_-, and it is shown in dashed red lines in Fig. 1a. The front propagation speed of the three fronts corresponding to discontinuities in $\rho(x,t)$ (shown in Fig. 1b) are equal to the slopes of different parts of $\tilde{Q}(\rho)$, as indicated in Fig. 1a.

Second, the SoC part of the solution can be derived by looking at the evolution of $\varepsilon(x,t)$ along the trajectories of individual vehicles, given initial conditions (14). According to the derivation done in Section II-B, the SoC along the trajectories of individual vehicles (4) evolves according to

$$\frac{\mathrm{d}\varepsilon(x_\xi(t),t)}{\mathrm{d}t}=d(x_\xi(t),t).$$

As a consequence, the SoC $\varepsilon(x,t)$ is continuous along the trajectories $x_\xi(t)$ for all $x_\xi(0)$, and $\varepsilon(x,t)$ can only have discontinuities where the trajectories of vehicles are parallel to one of the fronts.

The resulting SoC $\varepsilon(x,t)$ is piecewise-linear in space and time, and has either n or $n+1$ fronts, depending on whether $\lambda_n=\lambda_{n+1}$ or not. The propagation speed λ_{n+1} is given as the traffic speed at density ρ_+,

$$\lambda_{n+1}=v_+=\mathcal{V}(\rho_+).$$

In case $\lambda_n=\lambda_{n+1}$, the part of $\varepsilon(x,t)$ defined for $\lambda_n t<x<\lambda_{n+1}t$ vanishes, and $\varepsilon(x,t)$ effectively has n fronts. In the example in Fig. 1, it can be seen that the description of $\varepsilon(x,t)$ has one front more than that of $\rho(x,t)$, i.e., that there is no discontinuity in $\rho(x,t)$ along $x=\lambda_{n+1}=v_+t$ for $t>0$.

Due to assumption (12), the speed of vehicles at (x,t) is never less than the slope of the characteristics of (1). Consequently, the SoC is continuous across all fronts i for which $\lambda_i<v_i$, where $v_i=\mathcal{V}(\rho_i)$. Therefore, the remaining parameters of $\varepsilon(x,t)$, ε_i, θ_i, and χ_i, $i=1,\dots,n+2$, are given by

$$\varepsilon_i=\begin{cases}\varepsilon_-, & i=1,\dots,n\\ \varepsilon_-, & i=n+1,\lambda_{n+1}>\lambda_n,\\ \varepsilon_+, & i=n+2,\end{cases}\quad \chi_i=\begin{cases}\chi_-, & i=1,\\ \vec{\chi}_{i-1}, & i=2,\dots,n,\\ \vec{\chi}_{i-1}, & i=n+1,\lambda_{n+1}>\lambda_n,\\ \chi_+, & i=n+2,\end{cases}\quad \theta_i=\begin{cases}d_-, & i=1,\\ d_i-\chi_i(v_i-\lambda_{i-1}), & i=2,\dots,n,\\ d_i-\chi_i(v_i-\lambda_{i-1}), & i=n+1,\lambda_{n+1}>\lambda_n,\\ d_+, & i=n+2,\end{cases}$$

where $d_i=\mathcal{D}(v_i)$, and we recursively define

$$\vec{\chi}_i=\frac{d_{i+1}-d_i+\chi_i(v_i-\lambda_i)}{v_{i+1}-\lambda_i}.$$

B. Generalized case

In order to be able to model situations when there are zones of the road with different features, as well as when there are ramp flows, we also study a more general case of the Riemann-like problem. First, we redefine functions Q and $\mathcal{D}$ to allow them to be defined piecewise in space and time,

$$q(x,t)=Q(\rho(x,t),x,t), \tag{17}$$

$$d(x,t) = \mathcal{D}(v(x,t),x,t), \tag{18}$$

with the boundaries between zones where $Q(\rho,x,t)$ and $\mathcal{D}(v,x,t)$ are defined by different flux and dissipation functions $Q_j(\rho)$ and $\mathcal{D}_j(v)$ in different zones, with the boundaries between these zones propagating at constant speed. We denote these boundary propagation speeds by Λ, and consider functions

$$Q(\rho,x,t) = \begin{cases} Q_{-}(\rho), & x < \Lambda t, \\ Q_{+}(\rho), & x > \Lambda t, \end{cases} \quad \mathcal{D}(v,x,t) = \begin{cases} \mathcal{D}_{-}(v), & x < \Lambda t, \\ \mathcal{D}_{+}(v), & x > \Lambda t, \end{cases}$$

in the generalized case of the Rieman-like problem. Furthermore, we assume that $\Lambda < v_{+}$, allow the possibility of an off-ramp flow r_{-}^{off} exiting the road immediately upstream of the boundary $x = \Lambda t$, and an on-ramp flow r_{+}^{on} entering the road immediately downstream of the boundary, with the SoC of the vehicles entering the road from the on-ramp evolving as

$$\varepsilon^{\text{on}}(t) = \varepsilon_{+}^{\text{on}} + \theta_{+}^{\text{on}} t, \quad t \geq 0.$$

On- and off-ramp flows are included in the generalized Riemann-like problem by adding a point source term to equations (1) and (10),

$$\frac{\partial \rho}{\partial t} + \frac{\partial q}{\partial x} = \delta(x - \Lambda t)(r_{+}^{\text{on}} - r_{-}^{\text{off}}), \tag{19}$$

$$\frac{\partial \rho\varepsilon}{\partial t} + \frac{\partial (v\rho\varepsilon)}{\partial x} = \rho d + \delta(x - \Lambda t)\left(r_{+}^{\text{on}}(\varepsilon_{+}^{\text{on}} + \theta_{+}^{\text{on}} t) - r_{-}^{\text{off}}\varepsilon((\Lambda t)-, t)\right). \tag{20}$$

Note that here we express the SoC dynamics in terms of normalized energy $\rho\varepsilon$, for ease of formulation of the influence of the on-ramp flow. We assume that r_{-}^{off} is such that

$$r_{-}^{\text{off}} = Q_{-}(\rho) - \Lambda\rho$$

has a solution on $\rho \in [0, \sigma_{m^{Q_{-}}}^{Q_{-}}]$, and that r_{+}^{on} is such that

$$r_{+}^{\text{on}} = Q_{+}(\rho) - \Lambda\rho$$

has a solution on $\rho \in [0, \sigma_{m^{Q_{+}}}^{Q_{+}}]$, where $\sigma_{m^{Q_{\pm}}}^{Q_{\pm}} = \sup \operatorname{supp} Q_{\pm}$ are the jam densities, i.e., the suprema of traffic densities for which $Q_{\pm}(\rho) > 0$.

The traffic density solution to this Riemann-like problem is given in two parts: zone $x < \Lambda t$, with flux function $Q_{-}(\rho)$, from ρ_{-} to ρ'_{-}, and zone $x > \Lambda t$, with flux function $Q_{+}(\rho)$, from ρ'_{+} to ρ_{+}. We denote the parameters of these solutions by superscript Q_{-} and Q_{+}, respectively. Traffic densities at the boundary ρ'_{-} and ρ'_{+} are given as maximizers of

$$\begin{aligned} \underset{\rho'_{-},\rho'_{+}}{\text{maximize}} \quad & Q_{+}(\rho'_{+}) - r_{+}^{\text{on}} - \Lambda\rho'_{+} \\ \text{s.t.} \quad & Q_{+}(\rho'_{+}) - r_{+}^{\text{on}} - Q_{-}(\rho'_{-}) + r_{-}^{\text{off}} = \Lambda(\rho'_{+} - \rho'_{-}) \\ & \tilde{V}_i^{Q_{-}} < \Lambda, \quad i = 0, \dots n^{Q_{-}} - 1, \\ & \tilde{V}_i^{Q_{+}} > \Lambda, \quad i = 0, \dots n^{Q_{+}} - 1, \end{aligned} \tag{21}$$

maximizing the flow over the boundary between the two flux functions, under specified constraints. The first constraint is a modification of the Rankine-Hugoniot condition (16), with added terms r_{+}^{on} and r_{-}^{off} representing ramp flows. The second and third constraints ensure that the solutions to Riemann-like problems in zones described by $Q_{-}(\rho)$ and $Q_{+}(\rho)$ only have fronts within their respective zones. Additionally, we assume that r_{-}^{off} is such that there exist at least one pair (ρ'_{-}, ρ'_{+}) for which all constraints are satisfied.

Alternatively, the ramp flows can be defined as additional constraints, in which case r_{+}^{on} and r_{-}^{off} are optimization variables. For example, the case when we want to model that a ratio of β_{-}^{off} of the mainstream flow leaves the road via an off-ramp is captured by imposing $r_{-}^{\text{off}} = \beta_{-}^{\text{off}} Q_{-}(\rho'_{-})$ as an additional constraint. Similarly, the case when the mainstream flow is prioritized and only as much on-ramp flow enters the road as can be supported by road capacity is captured by imposing $r_{+}^{\text{on}} = \min\{r_{+}^{\text{on,max}}, q_{+}^{\max} - Q_{+}(\rho'_{+})\}$, where $r_{+}^{\text{on,max}}$ is the maximum on-ramp flow in case it is not restricted by the conditions on the road, and $q_{+}^{\max}$ is the capacity of the road. Note that in this case, solving (21) can be more complex than in the case when r_{+}^{on} and r_{-}^{off} are given as constants, depending on the type of additional constraints. For simplicity, in this work, we assume that on- and off-ramp flows are given as piecewise-constant inputs to the system, although they may be externally defined to depend on the traffic state in some way, resulting in constant r_{+}^{on} and r_{-}^{off} in generalized Riemann-like problems.

The solution $\rho(x,t)$, $\varepsilon(x,t)$ is again in form (15), with different parameters. The parameters of $\rho(x,t)$ are given by the parameters of the solutions in zones described by $Q_{-}(\rho)$ and $Q_{+}(\rho)$,

$$\rho_i = \begin{cases} \rho_i^{Q_{-}}, & i = 1, \dots, n^{Q_{-}} + 1, \\ \rho_{i-n^{Q_{-}}-1}^{Q_{+}}, & i = n^{Q_{-}} + 2, \dots, n+1, \end{cases} \quad \lambda_i = \begin{cases} \lambda_i^{Q_{-}}, & i = 1, \dots, n^{Q_{-}}, \\ \Lambda, & i = n^{Q_{-}} + 1, \\ \lambda_i^{Q_{+}}, & i = n^{Q_{-}} + 2, \dots, n, \end{cases}$$

with $n = n^{Q_-} + n^{Q_+} + 1$, as explained in more detail in [20]. Following the notation from Section III-A, the column vector of $\rho_i^{Q_-}$, $i = 1, \ldots, n^{Q_-} + 1$, is given by ${}^{\rho_-}\tilde{\Sigma}^{\rho'_-}_{Q_-}$, and the column vector of $\rho_i^{Q_+}$, $i = 1, \ldots, n^{Q_+} + 1$ by ${}^{\rho'_+}\tilde{\Sigma}^{\rho_+}_{Q_+}$. The parameters of $\varepsilon(x,t)$ are

$$\varepsilon_i = \begin{cases} \varepsilon_-, & i = 1, \ldots, n^{Q_-} + 1, \\ \vec{\varepsilon}_-, & i = n^{Q_-} + 2, \ldots, n, \\ \vec{\varepsilon}_-, & i = n+1, \lambda_{n+1} > \lambda_n, \\ \varepsilon_+, & i = n+2, \end{cases} \qquad \chi_i = \begin{cases} \chi_-, & i = 1, \\ \vec{\chi}_{i-1}, & i = 2, \ldots, n, \\ \vec{\chi}_{i-1}, & i = n+1, \lambda_{n+1} > \lambda_n, \\ \chi_+, & i = n+2, \end{cases}$$

where $\vec{\varepsilon}_-$ is defined as

$$\vec{\varepsilon}_- = \frac{(\rho_{n^{Q_-}+1}(v_{n^{Q_-}+1} - \Lambda) - r_-^{\text{off}})\varepsilon_- + r_+^{\text{on}}\varepsilon_+^{\text{on}}}{\rho_{n^{Q_-}+2}(v_{n^{Q_-}+2} - \Lambda) - r_-^{\text{off}} + r_+^{\text{on}}}, \tag{22}$$

and $\vec{\chi}_i$ are redefined to

$$\vec{\chi}_i = \begin{cases} \frac{d_{i+1} - d_i + \chi_i(v_i - \lambda_i)}{v_{i+1} - \lambda_i}, & i = 1, \ldots, n^{Q_-}, n^{Q_-}+2, \ldots, n+1, \\ \frac{d_{i+1}\rho_{i+1}(v_{i+1} - \lambda_i) - (d_i - \chi_i(v_i - \lambda_i))\left(\rho_i(v_i - \lambda_i) - r_-^{\text{off}}\right) - r_+^{\text{on}}\theta_+^{\text{on}}}{\rho_{i+1}(v_{i+1} - \lambda_i)^2}, & i = n^{Q_-} + 1. \end{cases} \tag{23}$$

The expressions for v_i and d_i now depend on whether the zone that they describe is upstream or downstream of the boundary $x = \Lambda t$,

$$v_i = \begin{cases} \frac{Q_-(\rho_i)}{\rho_i}, & i = 1, \ldots, n^{Q_-} + 1, \\ \frac{Q_+(\rho_i)}{\rho_i}, & i = n^{Q_-} + 2, \ldots, n+1, \end{cases}, \quad d_i = \begin{cases} \mathcal{D}_-(v_i), & i = 1, \ldots, n^{Q_-} + 1, \\ \mathcal{D}_+(v_i), & i = n^{Q_-} + 2, \ldots, n+1. \end{cases}.$$

IV. Front-tracking transition system model with advected energy

Having solved the Riemann-like problem of the CTE model in the previous section, we are now able to tackle the more general case and formulate the front-tracking solution and the front-tracking transition system form of the model. In this section, after specifying all aspects of the studied CTE model, we first provide its front-tracking solution, and then, based on that solution, formulate the Front-tracking Transition System Model with advected energy (FTSM+E), with equivalent behaviour. This model is an extension of the FTSM given in [20], including the advected energy and on- and off-ramp dynamics. We first present the transition system states, and then its transitions.

We study the CTE model (1), (8), where q is given by (17), v by (3), and d by (18). Let the initial conditions $\rho(x,0)$ and $\varepsilon(x,0)$ be

$$\rho(x,0) = \begin{cases} \rho_1, & x < x_1^\rho, \\ \vdots & \\ \rho_i, & x_{i-1}^\rho < x < x_i^\rho, \\ \vdots & \\ \rho_{N^\rho}, & x > x_{N^\rho - 1}^\rho, \end{cases} \qquad \varepsilon(x,0) = \begin{cases} \varepsilon_1, & x < x_1^\varepsilon, \\ \varepsilon_2 + \chi_2\left(x - x_1^\varepsilon\right), & x_1^\varepsilon < x < x_2^\varepsilon, \\ \vdots & \\ \varepsilon_i + \chi_i\left(x - x_{i-1}^\varepsilon\right), & x_{i-1}^\varepsilon < x < x_i^\varepsilon, \\ \vdots & \\ \varepsilon_{N^\varepsilon - 1} + \chi_{N^\varepsilon - 1}\left(x - x_{N^\varepsilon - 2}^\varepsilon\right), & x_{N^\varepsilon - 2}^\varepsilon < x < x_{N^\varepsilon - 1}^\varepsilon, \\ \varepsilon_{N^\varepsilon}, & x > x_{N^\varepsilon - 1}^\varepsilon, \end{cases} \tag{24}$$

with piecewise-constant traffic density and piecewise-linear SoC. We allow different zones of the road to have different traffic and energy dynamics, by defining the flux function Q and discharge function $\mathcal{D}$ piecewise in space and time,

$$Q(\rho, x, t) = Q_{\xi(x,t)}(\rho), \qquad \mathcal{D}(v, x, t) = \mathcal{D}_{\xi(x,t)}(v) \tag{25}$$

where $\xi(x,t) \in \mathbb{Z}$ denotes the unique identifier of each zone, given by the identifier function

$$\xi(x,t) = \left.\begin{cases} \xi_1^K, & x < x_1^{\xi,K} + \Lambda_1^{\xi,K}(t - T^K), \\ \vdots & \\ \xi_i^K, & x_{i-1}^{\xi,K} + \Lambda_{i-1}^{\xi,K}(t - T^K) < x < x_i^{\xi,K} + \Lambda_i^{\xi,K}(t - T^K), \\ \vdots & \\ \xi_{N^{\xi,K}}^K, & x > x_{N^{\xi,K}-1}^{\xi,K} + \Lambda_{N^{\xi,K}-1}^{\xi,K}(t - T^K), \end{cases}\right\}, T^K < t < T^{K+1}, \tag{26}$$

with $(\forall K)\, T^{K+1} > T^K, \xi_i^K \neq \xi_{i+1}^k, , i = 1, \ldots, N^{\xi,K} - 1$, each flux function $Q_\xi(\rho)$ is defined as (11) and satisfies (12), and there are no further constraints on discharge functions $\mathcal{D}_\xi(v)$.

Additionally, each zone defined by (26) potentially has traffic flow exiting the road via an off-ramp at its upstream boundary at piecewise-constant rate $r_i^{\text{off},K}$, and traffic flow entering the road via an on-ramp at its downstream boundary at piecewise-constant rate $r_i^{\text{on},K}$, with piecewise-linear SoC of the entering vehicles $\varepsilon_i^{\text{on},K} + \theta_i^{\text{on},K}(t - T^K)$ defined by $\varepsilon_i^{\text{on},K}$ and $\theta_i^{\text{on},K}$.

A. Front-tracking solution

Front-tracking [31] is a numerical approach for finding approximate solution to conservation laws, long used in traffic modelling [22], [32]. It relies on tracking the behaviour of the discontinuities (fronts) of the solution, while its behaviour between the discontinuities is described analytically or using other numerical methods. The method consists of approximating the flux function as piecewise-linear, approximating the initial conditions as piecewise-constant, solving the Riemann problems at all discontinuities, using the solution to describe the propagation of fronts, and finally, solving new Riemann problems that arise from collisions of two fronts. Note that the only step where approximations are introduced is at the beginning, after which the front-tracking method yields exact solutions to the approximated problem. Therefore, we are able to tune the level of approximation by choosing e.g., the number of flux function breakpoints and initial value discontinuities. In the case we study, both the flux functions and the initial conditions are such that no approximations need to be made, and front-tracking produces the exact solution.

Furthermore, considering the solution to the generalized Riemann-like problem presented in Section III-B, we see that the solution to the CTE model around a discontinuity, with piecewise-constant initial traffic density (13) and piecewise-linear SoC (14), also consists of piecewise-constant traffic density and piecewise-linear SoC (15). Therefore, we are also able to quantify the form of the solution to the model given a more general form of initial conditions (24) through the following Theorem.

Theorem 1. *Consider the CTE model* (1), (8)*, where q is given by* (17)*, v by* (3)*, and d by* (18)*, with initial conditions* (24)*, and functions $Q(\rho,x,t)$ and $\mathcal{D}(v,x,t)$ given by* (25)*, according to identifier function ξ given as* (26)*. Then the solution to the model consists of piecewise-constant traffic density $\rho(x,t)$ and piecewise-linear SoC $\varepsilon(x,t)$ for $t\geq 0$, of the form*

$$\rho(x,t)=\begin{cases}\rho_1^k, & x<z_1^k+\lambda_1^k(t-t^k),\\ \quad\vdots & \\ \rho_i^k, & z_{i-1}^k+\lambda_{i-1}^k(t-t^k)<x<z_i^k+\lambda_i^k(t-t^k),\\ \quad\vdots & \\ \rho_{n^{k_+}1}^k, & x>z_{n^k}^k+\lambda_{n^k}^k(t-t^k),\end{cases}\Bigg\},\ t^k<t<t^{k+1}, \tag{27}$$

$$\varepsilon(x,t)=\begin{cases}\varepsilon_1^k+\theta_1^k(t-t^k), & x<z_1^k+\lambda_1^k(t-t^k),\\ \varepsilon_2^k+\theta_2^k(t-t^k)+\chi_2^k\left(x-z_1^k-\lambda_1^k(t-t^k)\right), & z_1^k+\lambda_1^k(t-t^k)<x<z_2^k+\lambda_2^k(t-t^k),\\ \quad\vdots & \\ \varepsilon_i^k+\theta_i^k(t-t^k)+\chi_i^k\left(x-z_{i-1}^k-\lambda_{i-1}^k(t-t^k)\right), & z_{i-1}^k+\lambda_{i-1}^k(t-t^k)<x<z_i^k+\lambda_i^k(t-t^k),\\ \quad\vdots & \\ \varepsilon_{n^k}^k+\theta_{n^k}^k(t-t^k)+\chi_{n^k}^k\left(x-z_{n^k-1}^k-\lambda_{n^k-1}^k(t-t^k)\right), & z_{n^k-1}^k+\lambda_{n^k-1}^k(t-t^k)<x<z_{n^k}^k+\lambda_{n^k}^k(t-t^k),\\ \varepsilon_{n^{k_+}1}^k+\theta_{n^{k_+}1}^k(t-t^k), & x>z_{n^k}^k+\lambda_{n^k}^k(t-t^k),\end{cases}\Bigg\},t^k<t<t^{k+1}, \tag{28}$$

where $\chi_1^k=\chi_{n^{k_+}1}^k=0$,

$$(\forall K)(\forall j\in\{1,2,\dots,N^{\xi,K}-1\})\Big(\big(\exists k \text{ s.t. } t^k=T^K\big),\Big(\big(\forall k \text{ s.t. } [t^k,t^{k+1}]\cap[T^K,T^{K+1}]\neq\emptyset\big)\ \exists i \text{ s.t. } z_i^k=x_i^{\xi,K},\lambda_i^k=\Lambda_i^{\xi,K}\Big)\Big), \tag{29}$$

we have

$$\theta_i^k=\begin{cases}d_i^k, & i=1\vee i=n^k+1,\\ d_i^k-\chi_i^k(v_i^k-\lambda_{i-1}^k), & i=2,\dots,n^k,\end{cases} \tag{30}$$

v_i^k and d_i^k denote

$$v_i^k=\frac{\mathcal{Q}_{\xi_i^k}(\rho_i^k)}{\rho_i^k},\quad d_i^k=\mathcal{D}_{\xi_i^k}(v_i^k),$$

and ξ_i^k is the value of the identifier function $\xi(x,t)$ in zone $x\in[z_{i-1}^k+\lambda_{i-1}^k(t-t^k),z_i^k+\lambda_i^k(t-t^k)]$ for $t^k<t<t^{k+1}$.

Proof. The statement of the Theorem follows from the application of front-tracking. First, let $t^0=0-$, $t^1=0$, and $T^{K_0}\leq 0<T^{K_0+1}$. Then, the initial front positions z_i^0 are given as the values of the set $\{x_1^\rho,\dots,x_{n^\rho-1}^\rho\}\cup\{x_1^\varepsilon,\dots,x_{n^\varepsilon-1}^\varepsilon\}\cup\{x_1^{\xi,K_0},\dots,x_{n^{\xi,K_0}-1}^{\xi,K_0}\}$ sorted in an ascending order, $z_i^0>z_{i-1}^0$, $i=2,\dots,n^0$. Initial states ρ_i^0, ε_i^0, and χ_i^0, for $i=1,\dots,n^0+1$, are defined as

$$\rho_i^0=\begin{cases}\rho(z_i^0-,0), & i=1,\dots,n^0,\\ \rho(z_{i-1}^0+,0), & i=n^0+1,\end{cases}\quad \varepsilon_i^0=\begin{cases}\varepsilon(z_i^0+,0), & i=1,\\ \varepsilon(z_{i-1}^0+,0), & i=2,\dots,n^0+1,\end{cases}\quad \chi_i^0=\begin{cases}0, & i=1\vee i=n^0+1,\\ \frac{\partial\varepsilon(x,0)}{\partial x}\Big|_{x=z_i^0-}, & i=2,\dots,n^0.\end{cases}$$

First, for $k=0$, at each front z_i^k, we solve a Riemann-like problem with $\rho_-=\rho_i^k$, $\rho_+=\rho_{i+1}^k$, $\varepsilon_-=\varepsilon_i^k+\chi_i^k(x_i^k-x_{i-1}^k)$ if $i>1$ or $\varepsilon_-=\varepsilon_i^k$ if $i=1$, $\varepsilon_+=\varepsilon_{i+1}^k$, $\chi_-=\chi_i^k$, and $\chi_+=\chi_{i+1}^k$. The form of each solution is (15), which agrees with the form of the overall solution (27), (28). If $\xi(z_i^k-,t^k)=\xi(z_i^k+,t^k)$, the parameters of the solution are given in Section III-A.

Otherwise, for $\xi(z_i^k-,t^k) \neq \xi(z_i^k+,t^k)$, we define I_i^k through $z_i^k = x_{I_i^k}^{\xi,K_k} + \Lambda_{I_i^k}^{\xi,K_k}(t^k - T^{K_k})$, where K_k is defined through $T^{K_k} < t^k < T^{K_k+1}$, and the remaining parameters of the Riemann-like problem are

$$\Lambda = \Lambda_{I_i^k}^{\xi,K_k}, \quad Q_-(\rho) = Q_{\xi_{I_i^k}^{K_k}}(\rho), \quad Q_+(\rho) = Q_{\xi_{I_i^k}^{K_k}+1}(\rho), \quad \mathcal{D}_-(v) = \mathcal{D}_{\xi_{I_i^k}^{K_k}}(v), \quad \mathcal{D}_+(v) = \mathcal{D}_{\xi_{I_i^k}^{K_k}+1}(v),$$

the parameters of off-ramp flows r_-^{off} defined for zone $\xi_{I_i^k}^{K_k}$, and the parameters of on-ramp flows r_+^{on}, $\varepsilon_+^{\text{on}}$, and θ_+^{on} defined for zone $\xi_{I_i^k}^{K_k}+1$. In this case, the parameters of the solution are given in Section III-B. The parameters of the solutions to the Riemann-like problem at each discontinuity determine the updated states ρ_i^{k+1}, ε_i^{k+1}, and χ_i^{k+1}, for $i = 1,\dots,n^{k+1}+1$, which define the solution $\rho(x,t)$ and $\varepsilon(x,t)$ for $t^k < t < t^{k+1}$, until time t^{k+1} when either $t^{k+1} = T^{K_k+1}$ or two fronts collide,

$$z_j^k + \lambda_j^k(t^{k+1}-t^k) = z_{j+1}^k + \lambda_{j+1}^k(t^{k+1}-t^k), \quad \lambda_j^k > \lambda_{j+1}^k, \quad j \in \{1,\dots,n^k\}.$$

At time t^{k+1}, a new set of Riemann-like problems are solved, with parameters defined by $\rho(x,t^{k+1}-)$, $\varepsilon(x,t^{k+1}-)$, and with functions $Q(\rho,x,t^{k+1}+)$ and $\mathcal{D}(v,x,t^{k+1}+)$. These solutions define the new parameters ρ_i^{k+2}, ε_i^{k+2}, and χ_i^{k+2}, for $i = 1,\dots,n^{k+2}+1$, and the process repeats.

□

Statement (29) ensures that the discontinuities of the identifier function $\xi(x,t)$ always correspond with some fronts.

The form of $\varepsilon(x,t)$ given by (28) only allows discontinuities in space at the position of the fronts $z_i^k + \lambda_i^k(t-t^k)$, $t^k < t < t^{k+1}$. Additionally, due to the nature of the solutions to the Riemann-like problem studied in Section III, $\varepsilon(x,t)$ can only have discontinuities at the position of those fronts for which $v_i^k = \lambda_i^k$ and $v_{i+1}^k = \lambda_i^k$. Therefore, for all fronts i for which $v_i^k < \lambda_i^k$ and $v_{i+1}^k < \lambda_i^k$, we have

$$\varepsilon_i^k + \theta_i^k(t-t^k) + \chi_i^k(z_i^k + \lambda_i^k(t-t^k) - z_{i-1}^k - \lambda_{i-1}^k(t-t^k)) = \varepsilon_{i+1}^k + \theta_{i+1}^k(t-t^k), \quad t^k < t < t^{k+1}.$$

Substituting (30), we get that $\varepsilon_{i+1}^k = \vec{e}_i^k$ and $\chi_{i+1}^k = \vec{\chi}_i^k$, with $\vec{\varepsilon}_i^k$ given by

$$\vec{\varepsilon}_i^k = \frac{(\rho_i^k(v_i^k - \lambda_i^k) - r_i^{\text{off},k})(\varepsilon_i^k + \chi_i^k(z_i^k - z_{i-1}^k)) + r_{i+1}^{\text{on},k}\varepsilon_{i+1}^{\text{on},k}}{\rho_{i+1}^k\left(v_{i+1}^k - \lambda_i^k\right)}, \tag{31}$$

similarly to (22), and $\vec{\chi}_i^k$ by

$$\vec{\chi}_i^k = \frac{d_{i+1}^k\rho_{i+1}^k\left(v_{i+1}^k - \lambda_i^k\right) - \left(d_i^k - \chi_i^k\left(v_i^k - \lambda_i^k\right)\right)\left(\rho_i^k\left(v_i^k - \lambda_i^k\right) - r_i^{\text{off},k}\right) - r_{i+1}^{\text{on},k}\theta_{i+1}^{\text{on},k}}{\rho_{i+1}^k\left(v_{i+1}^k - \lambda_i^k\right)^2}, \tag{32}$$

similarly to (23), for all such fronts. For ease of notation, we will omit superscript k in further text wherever unambiguous.

B. FTSM formulation

The presented procedure of finding the front-tracking solution to the CTE model can be formulated as a transition system, forming a version of the FTSM. As opposed to the FTSM in [20], the model now also captures the SoC dynamics, and on- and off-ramp flows, and must therefore be augmented by the states and transitions related to them. Furthermore, all transitions need to be modified in order to account for the newly added states. In particular, the new states related to each zone are SoC at its upstream end ε, and the slope of the SoC in it χ. Flux functions are now generalized to also describe the energy dynamics of some zone of the road, through the discharge function $\mathcal{D}$, as well as flow r^{on} entering the road from an on-ramp at the upstream end of the zone, with initial SoC ε^{on} and rate of change of SoC θ^{on}, and flow r^{off} exiting the road via an off-ramp at the downstream end of the zone. Finally, a new SoC advection transition $\cup_i$ ensures that the SoC dynamics are modelled correctly. For completeness, in the remainder of this section, the entirety of the FTSM+E will be presented, including the parts from the FTSM presented in [20].

The set of states $\mathcal{X} = (n, t, \bar{z}, \bar{\rho}, \bar{\varepsilon}, \bar{\chi}, \bar{Q})$ is composed of:

- Number of active fronts: $n \in \mathbb{N}$,
- Time: $t \in \mathbb{R}_{\geq 0}$,
- Front positions: $z \in \mathbb{R}^{n_{\max}}$, $z_i \leq z_{i+1}$ for $i = 1,\dots,n_{\max}-1$,
- Traffic densities: $\rho \in \mathbb{R}_{\geq 0}^{n_{\max}+1}$,
- SoC at upstream end of the zone: $\varepsilon \in \mathbb{R}^{n_{\max}+1}$,
- SoC slope: $\chi \in \mathbb{R}^{n_{\max}+1}$,
- Generalized flux functions: $Q \in \mathcal{Q}^{n_{\max}+1}$, where $\mathcal{Q}$ is a set of generalized flux functions.

Each generalized flux function can be described by a quintuple $Q_* = (V, \Sigma, \mathcal{D}, \Lambda^{\pm}, \xi)$, consisting of:

- Slopes and breakpoints: $(V,\Sigma) \in \mathcal{L}$,
- Discharge function: $\mathcal{D} \in \mathbb{R}^{\mathbb{R}}$,
- Ramp flows: $(r^{\text{on}}, r^{\text{off}}) \in \mathbb{R}_{\geq 0}^2$,

- Initial on-ramp SoC: $\varepsilon^{\text{on}} \in \mathbb{R}$,
- Rate of change of on-ramp SoC: $\theta^{\text{on}} \in \mathbb{R}$,
- Boundary speeds: $\Lambda^{\pm} \in \mathbb{R}^2$,
- Identifier: $\xi \in \mathbb{Z}$,

where the set of feasible slopes and breakpoints is

$$\mathcal{L} = \left\{ V \in \mathbb{R}^m, \Sigma \in \mathbb{R}^{m+1}_{>0} : \sigma_1 < \sigma_2 < \ldots < \sigma_{m+1}, (\forall j < i)\ \sigma_i q^{\sigma}_{Q_*,j} > \sigma_j q^{\sigma}_{Q_*,i}, (i = 1, \ldots m)\ q^{\sigma}_{Q_*,i} \geq 0, q^{\sigma}_{Q_*,m+1} = 0 \right\},$$
$$q^{\sigma}_{Q_*,1} = V_1 \sigma_1, \quad q^{\sigma}_{Q_*,i} = q^{\sigma}_{Q_*,i-1} + V_i(\sigma_i - \sigma_{i-1}), i = 2, \ldots, m+1.$$

Same as in case of the FTSM presented in [20], we denote the traffic flow, given traffic density ρ, as $q = Q_*(\rho)$ and calculate it like $Q_j(\rho)$ in (11), with $V_{j,i}$ and $\sigma_{j,i}$ given in V and Σ, respectively. Boundary speeds $\Lambda^{\pm} = (\Lambda^{-}, \Lambda^{+})$ represent the propagation speed of the upstream and downstream boundary of the region of Q_*. The unique identifier ξ is used to differentiate between different flux functions, as well as to define the precedence when determining the propagation speed of the boundary between regions with different flux functions, e.g.., the propagation speed of the boundary between flux functions $Q_i \neq Q_{i+1}$, is given by

$$\lambda_i = \begin{cases} \Lambda^{+}_i, & \xi_i > \xi_{i+1}, \\ \Lambda^{-}_{i+1}, & \xi_i < \xi_{i+1}. \end{cases}$$

Flux functions from [20] are generalized to include the discharge function $\mathcal{D}$, as well as potential on- and off-ramp flows. For traffic density ρ and flux function Q_*, battery discharge rate is given as $d = \mathcal{D}(Q_*(\rho)/\rho)$. The on-ramp flow r^{on} enters the road immediately downstream of the upstream boundary of the zone described by generalized flux function Q_*, and the off-ramp flow r^{off} leaves the road immediately upstream of the downstream boundary of the zone. The SoC of the traffic entering the road is given by ε^{on} at current time t, and as time progresses, it changes at rate θ^{on}, such that it is $\varepsilon^{\text{on}} + \theta^{\text{on}}\tau$ at time $t + \tau$.

Given the current state $X^k \in \mathcal{X}$ of the transition system with time t^k, the traffic density $\rho(x,t)$ and SoC $\varepsilon(x,t)$, describing the state of the system for $t^k < t < t^{k+1}$ can be reconstructed based on $z^k_1, \ldots, z^k_{n^k}$, $\rho^k_1, \ldots, \rho^k_{n^k+1}$, $\varepsilon^k_1, \ldots, \varepsilon^k_{n^k+1}$, and $\chi^k_1, \ldots, \chi^k_{n^k+1}$, according to (27) and (28), with θ^k_i given by (30), ensuring that $\chi^k_1 = \chi^k_{n^k+1} = 0$ for all k by enforcing $\chi^0_1 = \chi^0_{n^0+1} = 0$ in the initial conditions.

As was the case for the FTSM [20], the model behaviour is described by defining its transitions $X \xrightarrow{\circ} X'$,where $\circ$ denotes any transition, X is the current state, and X' its successor state. In additions to passage of time $\tau(t_{\text{end}})$, front interaction $-_i$, internal Riemann $\sim_i$, and boundary Riemann $/_i$ transitions, which were a part of the FTSM [20], we need one additional transition to describe the energy dynamics: SoC advection transition $\cup_i$. Furthermore, all transitions need to be reformulated to include the updates of ε and χ.

The model dynamics can be split into the continuous and discrete part, corresponding to the hybrid system flow and jump behaviour, respectively, with the flow behaviour of the system described entirely by the passage of time transition, and all other transitions constituting jump behaviour. We ensure that the transition system model is deterministic by defining transition guard sets that form a partition of $\mathcal{X}$. All guard sets $\mathcal{G}_\circ$ are defined by some combination of the following conditions:

$$(\varepsilon_{j+1} = \vec{\varepsilon}_j) \wedge (\theta_{j+1} = \vec{\theta}_j) \wedge (\chi_{j+1} = \vec{\chi}_j),\ \text{if}\ (v_j > \lambda_j) \wedge (v_{j+1} > \lambda_j),\ j = 1, \ldots, n, \qquad (\star\cup)$$

$$(z_j < z_{j+1}) \vee \Big((z_j = z_{j+1}) \wedge \Big((\lambda_j < \lambda_{j+1}) \vee \big((\lambda_j = \lambda_{j+1}) \wedge (Q_j \neq Q_{j+1}) \big) \Big) \Big),\ j = 1, \ldots, n-1, \quad (\star-)$$

$$\Big((\rho_j \neq \rho_{j+1}) \wedge \Big({}^{\rho_j}\tilde{\Sigma}^{\rho_{j+1}}_{Q_j} = [\rho_j\ \rho_{j+1}]^{\top} \Big) \Big) \vee \Big((\vec{\varepsilon}_j \neq \varepsilon_{j+1}) \vee (\chi_j \neq \chi_{j+1}) \vee (\theta_j \neq \theta_{j+1}) \Big),\ \text{if}\ Q_j = Q_{j+1},\ j = 1, \ldots, n, \qquad (\star\sim)$$

$$(\rho_j = \rho'_-(\rho_j, \rho_{j+1}, Q_j, Q_{j+1})) \wedge (\rho_{j+1} = \rho'_+(\rho_j, \rho_{j+1}, Q_j, Q_{j+1})),\ \text{if}\ Q_j \neq Q_{j+1},\ j = 1, \ldots, n, \qquad (\star/)$$

where $\rho'_-(\rho_j, \rho_{j+1}, Q_j, Q_{j+1})$ and $\rho'_+(\rho_j, \rho_{j+1}, Q_j, Q_{j+1})$ are given as the optimizers from the generalized Riemann problem solution described in Section III-B. For example, as will be discussed below, the passage of time transition can only be taken if all of the listed conditions are satisfied, therefore we say that it has the lowest priority. We present the transitions in order of increasing priority (from requiring all conditions ($\star$) to be satisfied in order to be taken, to requiring the fewest conditions), omitting the states that do not change from the description.

*1) **Passage of time transition** $\tau(t_{\text{end}})$:* The first transition we describe is the passage of time, capturing the continuous dynamics of the system, and modelling the propagation of fronts between their interactions, or until the externally provided goal time t_{end}. This transition is taken if the state X is in guard set

$$X \in \mathcal{G}_\tau = \{ X \in \mathcal{X} | (\star\cup), (\star-), (\star\sim), (\star/), \quad \tau \in [0, \tau^*] \}.$$

The transition is defined by

$$(t, z, Q, \varepsilon) \xrightarrow{\tau(t_{\text{end}})} (t', z', Q', \varepsilon')$$
$$t' = t + \tau^*, \quad z' = z + \lambda\tau^*, \quad \varepsilon' = \varepsilon + \theta\tau^*, \quad \varepsilon^{\text{on}\prime} = \varepsilon^{\text{on}} + \theta^{\text{on}}\tau^*$$

where $\lambda = \begin{bmatrix}\lambda_1 & \dots & \lambda_n\end{bmatrix}^\top$, with the wave-speeds λ_i given by

$$\lambda_i = \begin{cases} \frac{Q_{i+1}(\rho_{i+1}) - Q_i(\rho_i)}{\rho_{i+1} - \rho_i}, & \xi_i = \xi_{i+1}, \rho_i \neq \rho_{i+1} \\ v_i, & \xi_i = \xi_{i+1}, \rho_i = \rho_{i+1} \\ \lambda_i^+, & \xi_i > \xi_{i+1}, \\ \lambda_{i+1}^-, & \xi_i < \xi_{i+1}, \end{cases}$$

and $\theta = \begin{bmatrix}\theta_1 & \dots & \theta_{n+1}\end{bmatrix}^\top$, given by (30). The update of Q is given through the update of the initial on-ramp SoC ε^{on} of each of the generalized flux functions. The maximum time shift τ^* is the minimum of the time for which condition $(\star-)$ is first violated,

$$\tau_z^* = \min\left\{ \frac{z_{i+1} - z_i}{\lambda_i - \lambda_{i+1}} \middle| z_{i+1} \geq z_i, \lambda_i > \lambda_{i+1}, i = 1, \dots, n-1 \right\}$$

and the time to specified goal time $\tau_{\text{end}}^* = t_{\text{end}} - t$, $\tau^* = \max\{0, \min\{\tau_z^*, \tau_{\text{end}}^*\}\}$, so if $t \geq t_{\text{end}}$, we have $X' = X$.

*2) **SoC advection transition** $\cup_i$:* This transitions results from the fact that $\varepsilon(x,t)$ is continuous in space wherever $v_i < \lambda_i$ and $v_{i+1} < \lambda_i$, and it is taken when the state is in guard set

$$X \in \mathcal{G}_{\cup_i} = \left\{ X \in \mathcal{X} | \neg(\star\cup)_i, (\star\cup)_j, j < i, (\star/), (\star\sim), (\star-) \right\}.$$

where by $\neg(\star\cup)_i$ we signify that the $j = i$-th condition in $(\star\cup)$ is violated. For all transitions $\circ \in \{\cup, -, \sim, /\}$, we write $X \in \mathcal{G}_\circ$ if $X \in \mathcal{G}_{\circ_i}$ for all i. The transition can be described by

$$(n, z, \rho, Q, \varepsilon, \chi) \xrightarrow{\cup_i} (n', z', \rho', Q', \varepsilon', \chi')$$

$$\begin{aligned} n' &= n+1, & z' &= \left[\begin{array}{ccc|c|ccc} z_1 & \dots & z_i & z_i & z_{i+1} & \dots & z_n \end{array}\right]^\top, \\ \rho' &= \left[\begin{array}{ccc|c|ccc} \rho_1 & \dots & \rho_i & \rho_{i+1} & \rho_{i+1} & \dots & \rho_{n+1} \end{array}\right]^\top, & Q' &= \left[\begin{array}{ccc|c|ccc} Q_1 & \dots & Q_i & Q_{i+1} & Q_{i+1} & \dots & Q_{n+1} \end{array}\right]^\top. \\ \varepsilon' &= \left[\begin{array}{ccc|c|ccc} \varepsilon_1 & \dots & \varepsilon_i & \vec{\varepsilon}_i & \varepsilon_{i+1} & \dots & \varepsilon_n \end{array}\right]^\top, & \chi' &= \left[\begin{array}{ccc|c|ccc} \chi_1 & \dots & \chi_i & \vec{\chi}_i & \chi_{i+1} & \dots & \chi_{n+1} \end{array}\right]^\top, \end{aligned}$$

where $\vec{\varepsilon}_i$ is given by (31), and $\vec{\chi}_i$ by (32).

*3) **Front interaction transition** $-_i$:* A front interaction transition is taken when the state is in guard set

$$X \in \mathcal{G}_{-_i} = \left\{ X \in \mathcal{X} | \neg(\star-)_i, (\star-)_j, j > i, (\star\sim), (\star/) \right\},$$

i.e., when two fronts collide. In case of $-_i$, the position of fronts i and $i+1$ becomes equal, $z_i = z_{i+1}$ while their distance is decreasing, $\lambda_i > \lambda_{i+1}$, or their distance remains zero away from boundaries between different generalized flux functions, $\lambda_i = \lambda_{i+1}$ and $Q_i = Q_{i+1}$. The front interaction transition corresponds to removing one front and one zone,

$$(n, z, \rho, Q, \varepsilon, \chi) \xrightarrow{-_i} (n', z', \rho', Q'\varepsilon', \chi')$$

$$\begin{aligned} n' &= n-1, & z' &= \left[\begin{array}{ccc|ccc} z_1 & \dots & z_i & z_{i+2} & \dots & z_n \end{array}\right]^\top, \\ \rho' &= \left[\begin{array}{ccc|ccc} \rho_1 & \dots & \rho_i & \rho_{i+2} & \dots & \rho_{n+1} \end{array}\right]^\top, & Q' &= \left[\begin{array}{ccc|ccc} Q_1 & \dots & Q_i & Q_{i+2} & \dots & Q_{n+1} \end{array}\right]^\top, \\ \varepsilon' &= \left[\begin{array}{ccc|ccc} \varepsilon_1 & \dots & \varepsilon_i & \varepsilon_{i+2} & \dots & \varepsilon_{n+1} \end{array}\right]^\top, & \chi' &= \left[\begin{array}{ccc|ccc} \chi_1 & \dots & \chi_i & \chi_{i+2} & \dots & \chi_{n+1} \end{array}\right]^\top, \end{aligned}$$

If $Q_i \neq Q_{i+2}$, this transition is likely to cause condition $(\star/)$ to be violated, and thus be followed by transition $/_i$.

*4) **Internal Riemann transition** $\sim_i$:* This transitions results from conditions corresponding to those of the Riemann problem given in Section III-A, and it is taken when the state is in guard set

$$X \in \mathcal{G}_{\sim_i} = \left\{ X \in \mathcal{X} | \neg(\star\sim)_i, (\star\sim)_j, j > i, (\star/), Q_i = Q_{i+1} \right\},$$

The transition can be described by

$$(n, z, \rho, Q, \varepsilon, \chi) \xrightarrow{\sim_i} (n', z', \rho', Q', \varepsilon', \chi')$$

$$\begin{aligned} n' &= n+m-2, \quad m = {}^{\rho_i}\tilde{m}_{Q_i}^{\rho_{i+1}} & z' &= \left[\begin{array}{ccc|c|ccc} z_1 & \dots & z_{i-1} & z_i \mathbb{1}_{m-1}^\top & z_{i+1} & \dots & z_n \end{array}\right]^\top, \\ \rho' &= \left[\begin{array}{ccc|c|ccc} \rho_1 & \dots & \rho_{i-1} & {}^{\rho_i}\tilde{\Sigma}_{Q_i,W}^{\rho_{i+1}\top} & \rho_{i+2} & \dots & \rho_{n+1} \end{array}\right]^\top, & Q' &= \left[\begin{array}{ccc|c|ccc} Q_1 & \dots & Q_{i-1} & Q_i \mathbb{1}_m^\top & Q_{i+2} & \dots & Q_{n+1} \end{array}\right]^\top, \\ \varepsilon' &= \left[\begin{array}{ccc|c|ccc} \varepsilon_1 & \dots & \varepsilon_{i-1} & \varepsilon_i \mathbb{1}_{m-1}^\top & \varepsilon_{i+1} & \dots & \varepsilon_n \end{array}\right]^\top, & \chi' &= \left[\begin{array}{ccc|c|ccc} \chi_1 & \dots & \chi_{i-1} & \chi_i \mathbb{1}_{m-1}^\top & \chi_{i+1} & \dots & \chi_n \end{array}\right]^\top. \end{aligned}$$

Depending on ρ_i and ρ_{i+1}, the number of active states can decrease (if $\rho_i = \rho_{i+1}$), increase, or stay the same. Note that this transition only updates the traffic density part of the state in accordance to the solution of the Riemann problem from Section III-A, and is therefore very likely to cause condition $(\star\cup)$ to be violated. Therefore, the SoC dynamics of the system will be handled by transition $\cup$ after other transitions modelling traffic density dynamics are executed.

*5) **Boundary Riemann transition** $/_i$:* This transition can occur at interfaces between zones with different generalized flux functions and reflects the traffic density part of the solution from Section III-B. It is taken when the state is in guard set

$$X \in \mathcal{G}_{/_i} = \left\{ X \in \mathcal{X} | \neg(\star/)_i, (\star/)_j, j > i, Q_i \neq Q_{i+1} \right\}.$$

The transition can be described by

$$(n, z, \rho, Q, \varepsilon, \chi) \xrightarrow{/_i} (n', z', \rho', Q', \varepsilon', \chi')$$

$$n' = n + m_- + m_+ - 2,\ m_- = {}^{\rho_i}\tilde{m}^{\rho'_-}_{Q_i},\ m_+ = {}^{\rho'_+}\tilde{m}^{\rho_{i+1}}_{Q_{i+1}}, \qquad z' = \left[\begin{array}{c|c|c} z_1 \ \dots \ z_{i-1} & z_i \mathbb{1}^\top_{m_-+m_+} & z_{i+1} \ \dots \ z_n \end{array}\right]^\top,$$

$$\rho' = \left[\begin{array}{c|c|c|c} \rho_1 \ \dots \ \rho_{i-1} & {}^{\rho_i}\tilde{\Sigma}^{\rho'_-\top}_{Q_i} & {}^{\rho'_+}\tilde{\Sigma}^{\rho_{i+1}\top}_{Q_{i+1}} & \rho_{i+2} \ \dots \ \rho_{n+1} \end{array}\right]^\top, \qquad Q' = \left[\begin{array}{c|c|c|c} Q_1 \ \dots \ Q_{i-1} & Q_i \mathbb{1}^\top_{m_-} & Q_{i+1} \mathbb{1}^\top_{m_+} & Q_{i+2} \dots Q_{n+1} \end{array}\right]^\top,$$

$$\varepsilon' = \left[\begin{array}{c|c|c|c} \varepsilon_1 \ \dots \ \varepsilon_{i-1} & \varepsilon_i \mathbb{1}^\top_{m_-} & \varepsilon_{i+1} \mathbb{1}^\top_{m_+} & \varepsilon_{i+2} \dots \varepsilon_{n+1} \end{array}\right]^\top, \qquad \chi' = \left[\begin{array}{c|c|c|c} \chi_1 \ \dots \ \chi_{i-1} & \chi_i \mathbb{1}^\top_{m_-} & \chi_{i+1} \mathbb{1}^\top_{m_+} & \chi_{i+2} \dots \chi_{n+1} \end{array}\right]^\top,$$

where densities $\rho'_- = \rho'_-(\rho_i, \rho_{i+1}, Q_i, Q_{i+1})$ and $\rho'_+ = \rho'_+(\rho_i, \rho_{i+1}, Q_i, Q_{i+1})$ are obtained by solving the optimization problem (21), with $\rho_- = \rho_i$, $\rho_+ = \rho_{i+1}$, $Q_- = Q_i$, and $Q_+ = Q_{i+1}$, including potential traffic flows to an off-ramp r_i^{off} and from an on-ramp r_{i+1}^{on}. Note that this transition is likely to cause condition $(\star\cup)$ to be violated, and thus be followed by a number of transitions $\cup_j$ and $-_{j+1}$ for some j, until condition $(\star\cup)$ is ultimately satisfied.

V. Model discretizations

While the formulation of the FTSM+E is intrinsically grid-free and event-based, i.e., not relying on space discretization and sampling in time, it is often convenient to acquire the finite-dimensional discrete-time state, e.g., in case we want to implement a discrete-time control law. It is nonetheless possible to use a simple instantiation of the FTSM+E as a Riemann problem solver to formulate a Godunov-like scheme for discretization of the model (1) and (10) (or equivalently, (19) and (20), in case there are on- and off-ramps) in space and time.

In this section, we present two cell-based discretizations of the CTE model. The first one is based on the direct implementation of the Godunov-like scheme, relying on the solutions to the generalized Riemann-like problem presented in Section III. The second one, approximated CTE model, uses a simplifying assumption that all EVs in a single cell discharge their batteries at the same rate every time step.

A. Implementation of a Godunov-like scheme

The Godunov scheme [17] is a well-known numerical scheme for finite-volume approximation of PDEs, which relies on splitting the space into cells, assuming the state is constant in each cell, solving Riemann problems at the cell boundaries, and then updating the discrete-time cell state according by averaging the Riemann problem solutions over the cells. Note that here we use a slight modification of the Godunov scheme, which we call Godunov-like, since state ε is not conserved, even in case $d = 0$ (when there is no battery discharge). Instead, we formulate a Godunov scheme for discretizing the traffic density ρ and the normalized energy $\rho\varepsilon$, from which we may readily acquire ε.

We discretize the space into cells of length L and time into time steps T, and assume that $L > (V_{\max} - V_{\min})T$, where $V_{\max}$ and $V_{\min}$ are the maximum and minimum slopes of all flux functions considered in the studied case, respectively. This condition ensures that the Courant-Friedrichs-Levy condition holds, as well as that fronts originating from the upstream and the downstream cell boundary at some time t cannot collide by time $t + T$. With a slight abuse of notation, the state of cell I at time step k consists of its traffic density $\underline{\rho}_I^k$ and its SoC $\underline{\varepsilon}_I^k$. We assume that the flux and discharge function can be piecewise-defined in space (due to e.g., varying road geometry) and time (due to e.g., traffic control measures such as Variable Speed Limits), but that the boundaries between zones where different functions $Q_j(\rho)$ and $\mathcal{D}_j(v)$ describe the traffic and SoC dynamics must coincide with the cell boundaries, yielding $\Lambda = 0$. Therefore, the traffic density and SoC dynamics in each cell I are described by a single generalized flux function, which we denote $\underline{Q}_I^k$. Additionally, we assume that on- and off-ramp positions also coincide with cell boundaries, and ascribe on- and off-ramp flows to the generalized flux function upstream and downstream of that boundary, respectively. The on-ramp flow entering the road at the upstream end of cell I is written $\underline{r}_{\text{on},I}^k$, and we write its SoC $\underline{\varepsilon}_I^{\text{on},k}$, and the off-ramp flow exiting the road from the downstream end of cell I is $\underline{r}_{\text{off},I}^k$.

The Riemann-like problems solved in the Godunov-like scheme at time step k are defined by initial conditions (13) with $\rho_- = \underline{\rho}_I^k$, $\rho_+ = \underline{\rho}_{I+1}^k$, (14) with $\varepsilon_- = \underline{\varepsilon}_I^k$, $\varepsilon_+ = \underline{\varepsilon}_{I+1}^k$ $\chi_- = \chi_+ = 0$, by discharge and flux functions, and by potential on- and

off-ramp flows defined by $\underline{Q}_I^k$ and $\underline{Q}_{I+1}^k$. We denote the solution to the Riemann-like problem at the boundary between cell I and cell $I+1$ at time step k as $\rho(x,T;I,k)$, $\varepsilon(x,T;I,k)$, and we have

$$\rho(x,T;I,k)=\begin{cases}\rho'_1, & x<\lambda'_1T,\\ \quad\vdots & \\ \rho'_i, & \lambda'_{i-1}T<x<\lambda'_iT,\\ \quad\vdots & \\ \rho'_{n'+1}, & x>\lambda'_{n'}T,\end{cases}\qquad \varepsilon(x,T;I,k)=\begin{cases}\varepsilon'_1+\theta'_1T, & x<\lambda'_1T,\\ \varepsilon'_2+\theta'_2T+\chi'_2\left(x-\lambda'_1T\right), & \lambda'_1T<x<\lambda'_2T,\\ \quad\vdots & \\ \varepsilon'_i+\theta'_iT+\chi'_i\left(x-\lambda'_{i-1}T\right), & \lambda'_{i-1}T<x<\lambda'_iT,\\ \quad\vdots & \\ \varepsilon'_{n'}+\theta'_{n'}T+\chi'_{n'}\left(x-\lambda'_{n'-1}T\right), & \lambda'_{n'-1}T<x<\lambda'_{n'}T,\\ \varepsilon'_{n'+1}+\theta'_{n'+1}T, & x>\lambda'_{n'}T.\end{cases}$$

Parameters ρ'_i, λ'_i, n', ε'_i, χ'_i, and θ'_i are obtained from the FTSM+E solution X' at time $t=T$, for initial state X^0 defined by

$$n^0=1,\quad t^0=0,\quad z^0=0,\quad \rho^0=\begin{bmatrix}\underline{\rho}_I^k & \underline{\rho}_{I+1}^k\end{bmatrix}^\top,\quad \varepsilon^0=\begin{bmatrix}\underline{\varepsilon}_I^k & \underline{\varepsilon}_{I+1}^k\end{bmatrix}^\top,\quad \chi^0=\mathbb{0}_2,\quad Q=\begin{bmatrix}\underline{Q}_I^k & \underline{Q}_{I+1}^k\end{bmatrix}^\top.$$

Due to the structure of the initial conditions, finding X' consists simply of taking some number of transitions $\cup_i$, $-_i$, $\sim_i$, and $/_i$ until we reach state $X^{0'}\in\mathcal{G}_\tau$. Afterwards, all states $X^{0''}$, $X^{0'}\xrightarrow{\tau(t_{\text{end}})}X^{0''}$, $\forall t_{\text{end}}>0$ will be $X^{0''}\in\mathcal{G}_\tau$, and we acquire X' as $X^{0'}\xrightarrow{\tau(T)}X'$, by advancing time to $t'=T$.

Finally, the updated traffic density $\underline{\rho}_I^{k+1}$ and SoC $\underline{\varepsilon}_I^{k+1}$, acquired by applying the Godunov-like scheme can be expressed as

$$\underline{\rho}_I^{k+1}=\underline{\rho}_I^k+\frac{T}{L}\left(\underline{q}_{I-}^k-\underline{q}_{I+}^k\right), \tag{34}$$

$$\underline{\rho}_I^{k+1}\underline{\varepsilon}_I^{k+1}=\underline{\rho}_I^k\left(\underline{\varepsilon}_I^k+\underline{d}_I^kT\right)+\frac{T}{L}\left(\underline{\phi}_{I-}^k-\underline{\phi}_{I+}^k\right), \tag{35}$$

where the battery discharge $\underline{d}_I^k$ is given by

$$\underline{d}_I^k=\underline{\mathcal{D}}_I^k\left(\frac{\underline{Q}_I^k(\underline{\rho}_I^k)}{\underline{\rho}_I^k}\right), \tag{36}$$

and we define

$$\underline{q}_{I-}^k=\int_0^\infty\rho(x,T;I-1,k)-\underline{\rho}_I^k\mathrm{d}x=\sum_{i=2}^{n'}(\rho'_i-\underline{\rho}_I^k)(\max\{0,\lambda'_i\}-\max\{0,\lambda'_{i-1}\})T,$$

$$\underline{q}_{I+}^k=\int_{-\infty}^0\underline{\rho}_I^k-\rho(x,T;I,k)\mathrm{d}x=\sum_{i=2}^{n'}(\underline{\rho}_I^k-\rho'_i)(\min\{0,\lambda'_i\}-\min\{0,\lambda'_{i-1}\})T,$$

$$\begin{aligned}\underline{\phi}_{I-}^k&=\int_0^\infty\rho(x,T;I-1,k)\varepsilon(x,T;I-1,k)-\underline{\rho}_I^k(\underline{\varepsilon}_I^k+\underline{d}_I^kT)\mathrm{d}x=\dots\\&=\sum_{i=2}^{n'}\left(\left(\varepsilon'_i+\left(\theta'_i+\chi'_i\frac{\max\{0,\lambda'_i\}-\max\{0,\lambda'_{i-1}\}-2\lambda'_{i-1}}{2}\right)T\right)-(\underline{\varepsilon}_I^k+\underline{d}_I^kT)\right)(\max\{0,\lambda'_i\}-\max\{0,\lambda'_{i-1}\})T,\end{aligned}$$

$$\begin{aligned}\underline{\phi}_{I+}^k&=\int_{-\infty}^0\underline{\rho}_I^k(\underline{\varepsilon}_I^k+\underline{d}_I^kT)-\rho(x,T;I,k)\varepsilon(x,T;I,k)\mathrm{d}x=\dots\\&=\sum_{i=2}^{n'}\left((\underline{\varepsilon}_I^k+\underline{d}_I^kT)-\left(\varepsilon'_i+\left(\theta'_i+\chi'_i\frac{\min\{0,\lambda'_i\}-\min\{0,\lambda'_{i-1}\}-2\lambda'_{i-1}}{2}\right)T\right)\right)(\min\{0,\lambda'_i\}-\min\{0,\lambda'_{i-1}\})T.\end{aligned}$$

It is also possible to paralelize the process of finding $\underline{q}_{I\pm}^k$ and $\underline{\phi}_{I\pm}^k$ by constructing initial conditions that take all cells into account, essentially taking (24) with $\rho_i^0=\underline{\rho}_I^k$, $\varepsilon_i^0=\underline{\varepsilon}_I^k$, $\chi_i^0=0$, $i=I$, with cell boundaries $x_i^{\rho,0}=x_i^{\varepsilon,0}=(i-1)L$, and with Q_i^0 reflecting $\underline{Q}_I^k$.

B. Approximated CTE model

The approximate CTE model presented here is based on the discretization of the CTEC model introduced in [14]. Since it is also based on a Godunov-like scheme, this model has the same structure as the Godunov-like scheme using FTSM+E, thus

all its states are defined the same way. The expressions for the updated traffic density $\underline{\rho}_I^{k+1}$ and SoC $\underline{\varepsilon}_I^{k+1}$ are (34)–(35), same as for the Godunov-like scheme. The difference is only in how $\underline{q}_{I-}^k$, $\underline{q}_{I+}^k$, $\underline{\phi}_{I-}^k$, and $\underline{\phi}_{I+}^k$ are defined:

$$\underline{q}_{I-}^k = \underline{q}_{I-1+}^k - \underline{r}_{\text{off},I-1}^k + \underline{r}_{\text{on},I}^k, \tag{37}$$

$$\underline{q}_{I+}^k = \min\left\{\underline{Q}_I^k(\min\{\underline{\rho}_I^k, \underline{\sigma}_{\max,I}^k\}), \underline{Q}_{I+1}^k(\max\{\underline{\rho}_{I+1}^k, \underline{\sigma}_{\max,I+1}^k\}) - \underline{r}_{\text{on},I+1}^k + \underline{r}_{\text{off},I}^k\right\}, \tag{38}$$

$$\underline{\phi}_{I-}^k = (\underline{q}_{I-1+}^k - \underline{r}_{\text{off},I-1}^k)(\underline{\varepsilon}_{I-1}^k + \underline{d}_{I-1}^k T) + \underline{r}_{\text{on},I}^k \underline{\varepsilon}_{\text{on},I}^k, \tag{39}$$

$$\underline{\phi}_{I+}^k = \underline{q}_{I+}^k(\underline{\varepsilon}_I^k + \underline{d}_I^k T), \tag{40}$$

with battery discharge $\underline{d}_I^k$ defined by (36), and where by $\underline{\sigma}_{\max,I}^k$ we denote the critical density of $\underline{Q}_I^k(\rho)$, i.e., the density at which it achieves its maximum value.

As will be shown in the simulations, the approximate model given here achieves similar results to the one based on the Godunov-like scheme using FTSM+E, despite being significantly numerically simpler and more straightforward to implement. Due to the properties of the Godunov scheme, the traffic density dynamics of this approximate model, given by (37) and (38), are exactly the same as that of the Godunov-like scheme using FTSM+E, and the only discrepancy is due to the simplified definition of (39) and (40). Essentially, the approximate model assumes that all EVs in each cell travel at the same speed $\underline{Q}_I^k(\underline{\rho}_I^k)/\underline{\rho}_I^k$ during the entirety of the time step, which ignores the possibility that they change their speeds as they enter zones of with different traffic densities. In case there are no on- or off-ramps, the approximate CTE model (34)–(35), (37)–(40) simplifies to

$$\begin{aligned}
\underline{\rho}_I^{k+1} &= \underline{\rho}_I^k + \frac{T}{L}\left(\underline{q}_{I-1}^k - \underline{q}_I^k\right), \\
\underline{\rho}_I^{k+1}\underline{\varepsilon}_I^{k+1} &= \underline{\rho}_I^k\left(\underline{\varepsilon}_I^k + \underline{d}_I^k T\right) + \frac{T}{L}\left(\underline{q}_{I-1}^k\left(\underline{\varepsilon}_{I-1}^k + \underline{d}_{I-1}^k T\right) - \underline{q}_I^k\left(\underline{\varepsilon}_I^k + \underline{d}_I^k T\right)\right), \\
\underline{q}_I^k &= \min\left\{\underline{Q}_I^k\left(\min\{\underline{\rho}_I^k, \underline{\sigma}_{\max,I}^k\}\right), \underline{Q}_{I+1}^k\left(\max\{\underline{\rho}_{I+1}^k, \underline{\sigma}_{\max,I+1}^k\}\right)\right\}.
\end{aligned}$$

VI. Simulation Example

Finally, we demonstrate the use of the model through an illustrative simulation example comparing three simulation models:

1) FTSM+E proposed in this work (grid-free and event-based), given in Section IV-B,
2) Godunov-like scheme using FTSM+E (discretized in space and time), given in Section V-A, and
3) Approximated CTE model, given in Section V-B.

These models are ordered by exactness, from exact (for continuous piecewise-linear flux functions) to more approximate, and by numerical burden, from the most complex to the simplest. We first describe the simulation scenario, and then proceed to compare the solutions acquired from the three considered simulation models.

A. Scenario

We compared the three simulation models on a synthetic example involving elements that showcase all of the features of FTSM+E. The simulation scenario is sketched in Fig. 2. Simulations were executed on a 100 km road, and the total simulation time is $t_{\text{end}} = 1$ h. The road is split into four zones: flat road from $x = 0$ km to $x = 50$ km, uphill road with $\alpha_{\text{up}} = 5\%$ slope from $x = 50$ km to $x = 70$ km, downhill road with $\alpha_{\text{down}} = -5\%$ slope from $x = 70$ km to $x = 90$ km, and flat road from $x = 90$ km to $x = 100$ km. There is a single off-ramp, at $x = 50$ km, at the boundary between the flat zone and the uphill zone, and a single on-ramp at $x = 90$ km, at the boundary between the downhill zone and the flat zone.

Due to different driving behaviours on steep uphill and downhill slopes, these zones will be described by different flux functions than the one that describes the flat road, as shown in Figure 3. We assume that the traffic flow follows the Greenshields flux function,

$$Q_{\text{flat}}(\rho) = V\left(\frac{\rho}{P} - \left(\frac{\rho}{P}\right)^2\right),$$

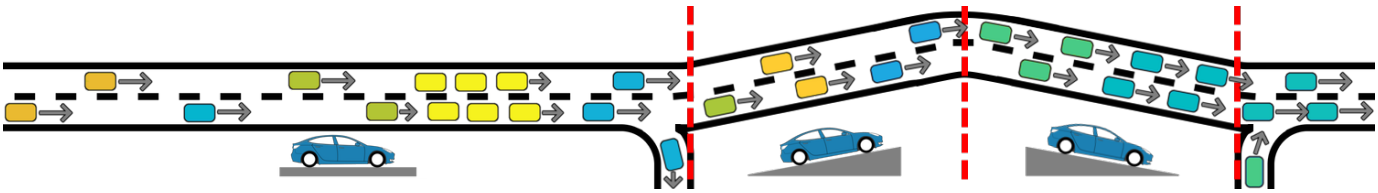

Fig. 2: A sketch of the simulation scenario. Initial traffic density is illustrated by the concentration of EVs, and their initial SoC is indicatively colour-coded (warmer is higher). Vertical dashed red lines denote boundaries between zones with different road grade.

where the free flow speed is $V = 100$ km/h in case of the flat road, and the jam density is $P = 60$ veh/km, resulting in critical density of $\sigma_{\max} = 30$ veh/km. We assume that the uphill and downhill zone flux functions are a scaled-down version of the flat road flux function, and follow the expressions used in [33], yielding

$$Q_{\text{up}}(\rho) = (1 + 3\alpha_{\text{up}} - 150\alpha_{\text{up}}^2)Q_{\text{flat}}(\rho) = 0.775Q_{\text{flat}}(\rho),$$
$$Q_{\text{down}}(\rho) = (1 - 5\alpha_{\text{down}} - 100\alpha_{\text{down}}^2)Q_{\text{flat}}(\rho) = 0.5Q_{\text{flat}}(\rho).$$

The flux functions were approximated as continuous and piecewise-linear, with $m = 15$ equally spaced breakpoints between $\rho = 0$ and $\rho = P$. Since the $Q_{\text{up}}(\rho) < Q_{\text{flat}}(\rho)$ and $Q_{\text{down}}(\rho) < Q_{\text{up}}(\rho)$ for $0 < \rho < P$, both of these zones will act as stationary bottlenecks.

Crucially, the uphill and downhill road segments will also translate into very different parameters of the battery discharge function. We assumed the battery discharge rate depends on the EV speed according to a third order polynomial,

$$\mathcal{D}_*(v) = D_0 + D_1^* v + D_2 v^2 + D_3 v^3.$$

In order to better illustrate the changes in SoC, we used quantities that are twice as large as the ones derived similarly to the battery discharge model in [9], assuming a 40 MWh battery capacity. Parameters $D_0 = -3.5{\cdot}10^{-2}$ 1/h, $D_2 = -3.28 \cdot 10^{-6}$ km^2/h^3, and $D_3 = -4.29 \cdot 10^{-7}$ km^3/h^4 do not depend on the slope of the road, and will therefore be the same for $\mathcal{D}_{\text{flat}}(v)$, $\mathcal{D}_{\text{up}}(v)$, and $\mathcal{D}_{\text{down}}(v)$. Parameter D_1^* models the energy expended to overcome an uphill road, or energy recovered from regenerative braking on a downhill road, thus it takes different values for the three cases, $D_1^{\text{flat}} = -1.67 \cdot 10^{-3}$ km/h^2, $D_1^{\text{up}} = -1.2 \cdot 10^{-2}$ km/h^2, and $D_1^{\text{down}} = 8.68 \cdot 10^{-3}$ km/h^2. Note that, as expected for such a steep uphill, D_1^{up} is almost an order of magnitude larger than D_1^{flat}, whereas for the considered steep downhill D_1^{down} is positive, meaning that the SoC of the vehicles on this road segment will be increasing in time for all but very low v.

We split the road into $n_{\text{cell}} = 10$ cells of $L = 10$ km length and adopt $T = 0.1$ h time step, respecting the CFL conditions. The initial conditions of the FTSM+E, $\rho(x, 0)$ and $\varepsilon(x, 0)$, were purposefully selected to illustrate the model features, and are shown in Figure 4. Since the cell-based simulation models can only represent piecewise-constant SoC, the initial $\underline{\varepsilon}_I^0$ were calculated as averages of $\varepsilon(x, 0)$ over their corresponding cells. The inflow into the first cell for the cell-based simulation models, $\underline{q}_{0+}^k$ and $\underline{\phi}_{0+}^k$, were selected to mirror the behaviour of the FTSM+E, essentially assuming that $\rho(x, t) = \rho(0, 0)$, and $\varepsilon(x, t) = \varepsilon(0, 0) + d(0, 0)t$, for $x < 0$. During the simulation, the off ramp flow at $x = 90$ km was set to $r^{\text{off}} = 400$ veh/h, and on-ramp flow at $x = 50$ km to $r^{\text{on}} = 800$ veh/h, with the SoC of the EVs entering the road via the on-ramp described by $\varepsilon^{\text{on}} = 0.5$ and $\theta^{\text{on}} = 0.4$ 1/h, resulting in the SoC of the on-ramp EVs being 0.5 at $t = 0$ h and 0.9 at $t = 1$ h.

B. FTSM+E solution

The FTSM+E simulation results are shown shown colour-coded in Figure reffig:ftsm, displaying the traffic density in Figure 5a, and the SoC in Figure 5b. Each zone defined by the fronts on its borders in Figure 5a is the same colour, whereas the zones in Figure 5b can have gradients in x and t, as expected from the form of the solution (27)–(28).

The vertical dashed red lines indicate positions where there is a boundary between zones described by different flux functions. At two of these boundaries, we also have off-ramp ($x = 50$ km) and on-ramp ($x = 90$ km) flows. The vertical dashed white lines indicate the boundaries of the cells, and horizontal dashed white lines the time steps that are used for the cell-based discrete-time models. Although these have no influence on the FTSM+E dynamics, they will be used to calculate average cell traffic density and SoC, which will be compared with those of the other models.

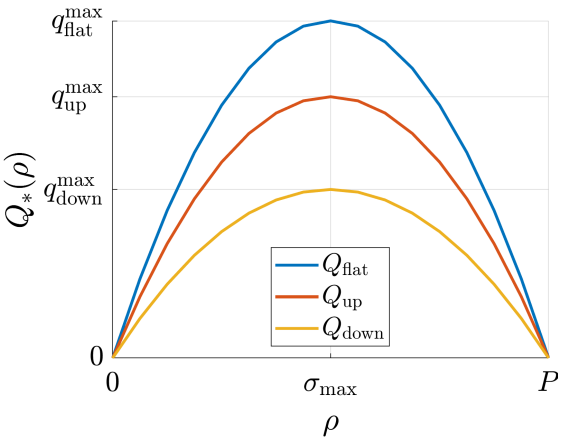

Fig. 3: Flux functions describing the traffic flow on flat, uphill, and downhill road.

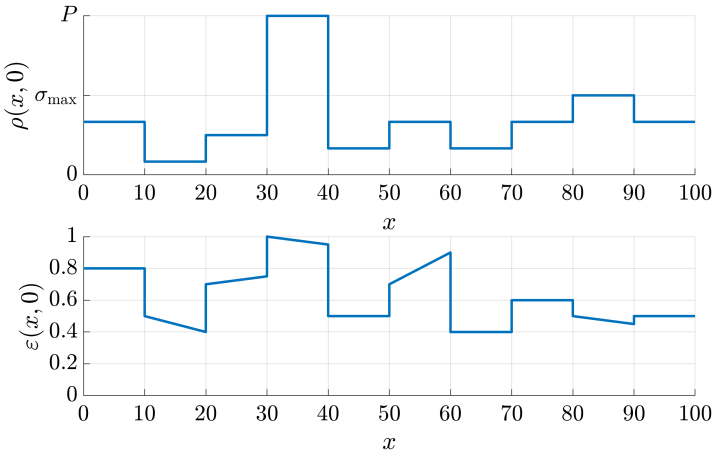

Fig. 4: Initial conditions $\rho(x, 0)$ and $\varepsilon(x, 0)$.

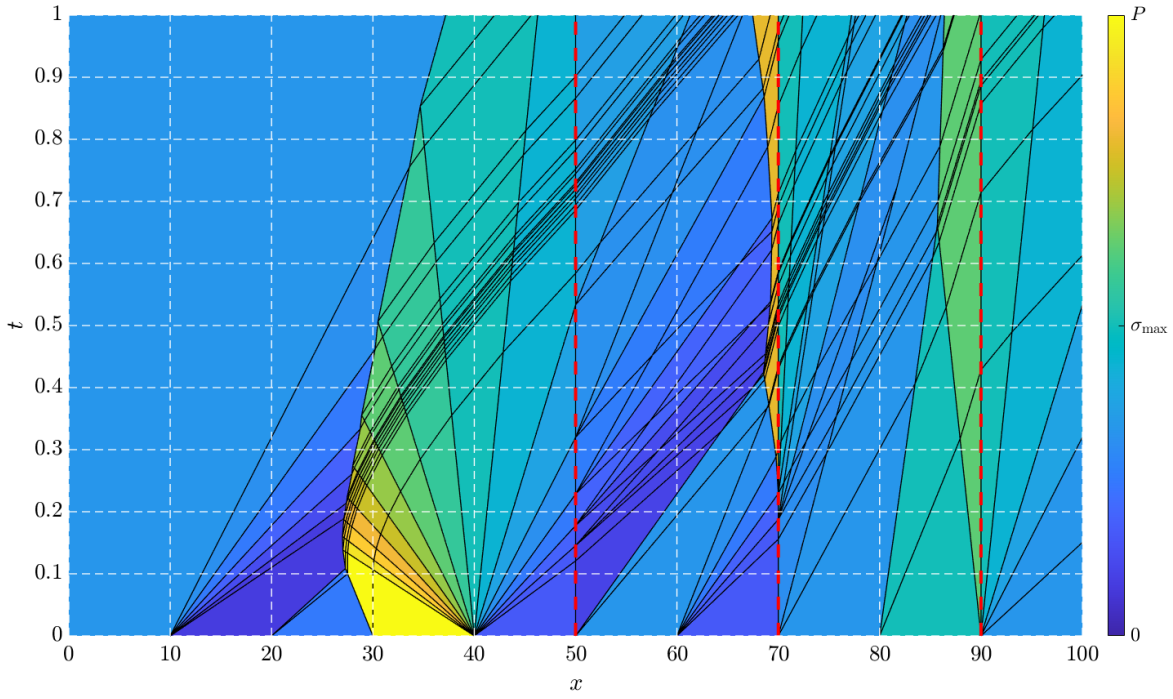

(a) Traffic density $\rho(x, t)$.

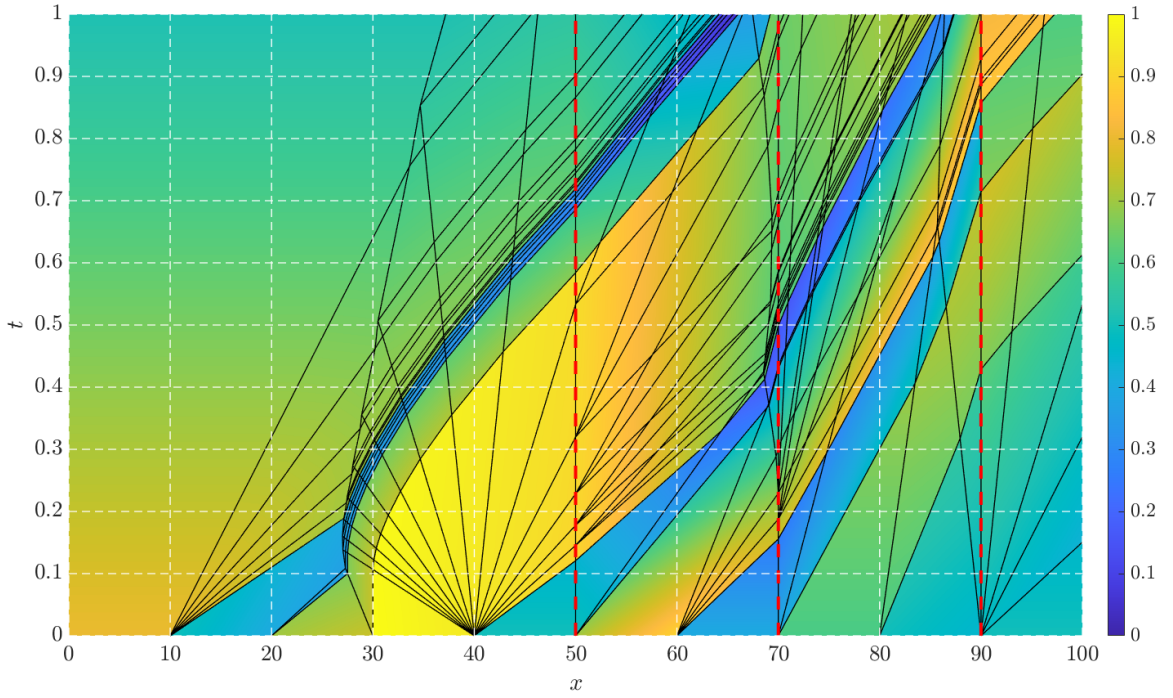

(b) State of charge $\varepsilon(x, t)$.

Fig. 5: The full FTSM+E solution for the given scenario.

It can be seen that the solution involves a large number of fronts, mostly as a result of having a fairly close approximation of the continuous flux function (see Figure 3), with a large number of breakpoints. This allows for a very detailed representation of both $\rho(x,t)$ and $\varepsilon(x,t)$, with no diffusion. The only place where there is a loss of information due to averaging SoC is at the on-ramp, due to the impossibility of representing two distinct groups of vehicles at the same position. Elsewhere, we may recover the SoC profile of individual EVs over time if we follow their trajectories, $\varepsilon_\xi(t) = \varepsilon(x_\xi(t), t)$. For example, in Figure 5b, it is possible to visually follow the trajectories of vehicles that were in $x \in [10, 20]$ km at $t = 0$, since their SoC is lower than that of the EVs upstream and downstream of them, $\varepsilon(x, 0) = 0.5 - 0.01(x - 10)$, $x \in [10, 20]$. At $t = 1$ h, these vehicles occupy $x \in [64.13, 66]$ km, and their SoC ranges approximately from 0.12 to 0.06.

As expected, the bottleneck at $x = 70$ km causes a new zone of congestion to arise around $t = 0.3$ h. Furthermore, the traffic flow from the on-ramp at $x = 90$ km also causes some lighter congestion to persist upstream of it throughout the simulation, since the initial traffic density in $x \in [80, 90]$ km is equal to the critical density. Finally, following the trajectories of the vehicles traversing the downhill road segment, it can be seen that their SoC does indeed increase in time, although this increase might not be obvious in Figure 5b.

C. Simulation model comparison

We can now compare the considered simulation models. A qualitative comparison of the simulation results is given in Figures 6 and 7, with cell-averaged discrete-time traffic density shown colour-coded in Figure 6, and cell-averaged discrete time SoC in Figure 7. The cell-averaged traffic density in Figure 6a is calculated by averaging the FTSM+E traffic density $\rho(x,t)$ over space

$$\underline{\rho}_I^k = \frac{1}{L} \int_{(I-1)L}^{IL} \rho(x, kT) \mathrm{d}x,$$

whereas the cell-averaged SoC in Figure 7a is calculated by averaging the FTSM+E SoC $\varepsilon(x,t)$ over the vehicles in the cell

$$\underline{\varepsilon}_I^k = \frac{1}{\underline{\rho}_I^k L} \int_{(I-1)L}^{IL} \rho(x, kT)\varepsilon(x, kT) \mathrm{d}x.$$

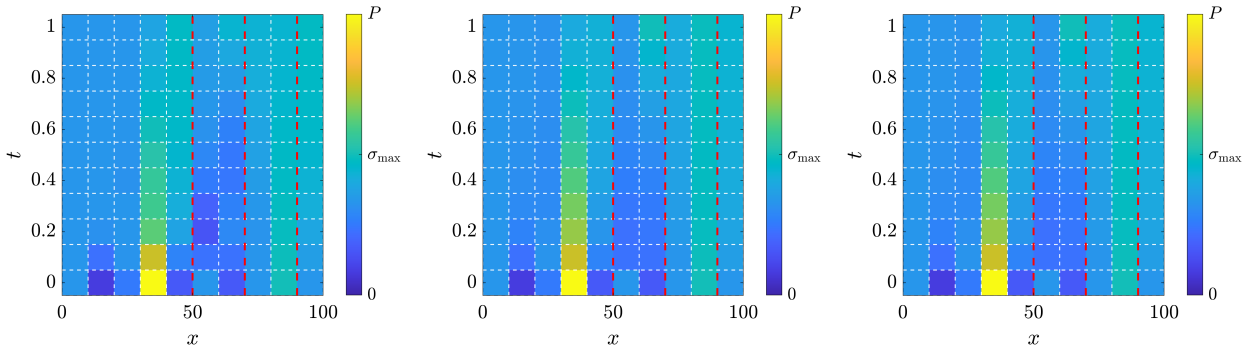

(a) FTSM+E (b) Godunov-like using FTSM+E (c) Approximate CTE

Fig. 6: Cell-averaged traffic densities for the three compared models.

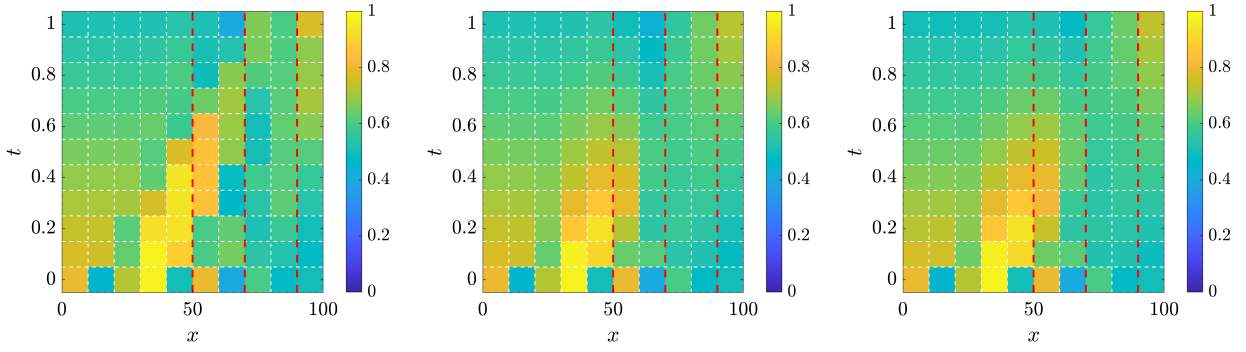

(a) FTSM+E (b) Godunov-like using FTSM+E (c) Approximate CTE

Fig. 7: Cell-averaged SoC for the three compared models.

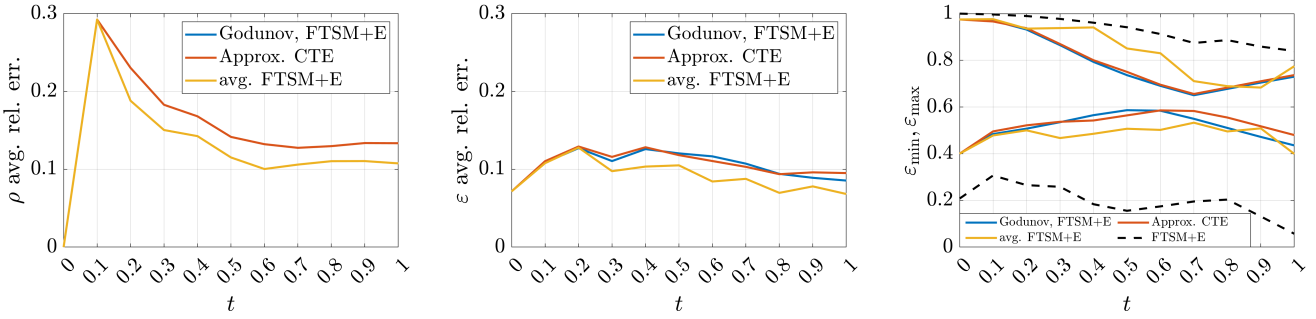

(a) Average relative error in ρ (b) Average relative error in ε (c) Minimum and maximum values of ε

Fig. 8: Quantitative comparison of the three used simulation models.

As expected, the cell-averaged traffic density of the Godunov-like scheme using FTSM+E and the approximated CTE model, shown in Figures 6b and 6c, are exactly the same. They are also very similar to the one corresponding to the exact FTSM+E solution, although a lot of the finer details of the traffic density spacetime profile is lost by averaging. The two cell-based models differ in how their SoC dynamics is defined, although they exhibit a very similar behaviour in the presented simulation example. Their SoC does deviate noticeably from its cell-averaged FTSM+E solution counterpart, and even more so from the exact FTSM+E solution.

A more quantitative comparison is given in Figure 8. First, we compare the average relative errors of the cell-averaged FTSM+E solution and the two cell-based models, with the exact FTSM+E solution taken as ground truth. Here the average relative errors are defined as

$$\mathrm{err}_{\underline{\rho}}^{k} = \frac{1}{n_{\mathrm{cell}}} \sum_{I=1}^{n_{\mathrm{cell}}} \frac{\int_{(I-1)L}^{IL} \left| \rho(x, kT) - \underline{\rho}_I^k \right| \mathrm{d}x}{\underline{\rho}_I^k},$$

$$\mathrm{err}_{\underline{\varepsilon}}^{k} = \frac{1}{n_{\mathrm{cell}}} \sum_{I=1}^{n_{\mathrm{cell}}} \frac{\int_{(I-1)L}^{IL} \left| \rho(x, kT)\varepsilon(x, kT) - \underline{\rho}_I^k \underline{\varepsilon}_I^k \right| \mathrm{d}x}{\underline{\rho}_I^k \underline{\varepsilon}_I^k},$$

and their comparison is given in Figures 8a and 8b. It can be seen that most of the error comes from averaging, since the cell-averaged FTSM+E solution seems to be consistently better by only about 0.025 after the first time step. Since the initial traffic density was in the form that can be accurately represented by $\underline{\rho}_I^0$, we can see that its error at $t = 0$ is zero. However, due to the initial SoC containing linear parts with non-zero slope, the error in SoC is greater than zero from the start.

Finally, an important property of the FTSM+E solution is that it preserves the SoC information on a practically per-vehicle basis, whereas some information is lost due to averaging in case of cell-based models. To illustrate this, in Figure 8c we show a comparison of the minimum and maximum SoC sampled at times $t = kT$. It can be seen that, at least in this example, all cell-averaged models demonstrate a significantly narrower range of SoC compared to the exact FTSM+E solution, with the cell-averaged FTSM+E solution achieving only slightly better results than the two cell-based models. In this example, this is due to the fact that there was a cell with low traffic density and low SoC in the initial conditions. The EVs from this cell were immediately absorbed into the nearby traffic, and the information about their SoC was effectively lost.

VII. Conclusion

In summary, in this work we study a macroscopic EV traffic model that includes the flows of energy carried in their batteries, consisting of a conservation law coupled with an advection equation. We define and solve a generalized form of Riemann problem for this model, allowing for piecewise linear initial SoC, piecewise-defined flux function, and on- and off-ramp flows. Based on this solution, we formulate FTSM+E, which can be used to obtain exact solutions for the specific case when flux functions are continuous and piecewise-linear. Finally, we use an illustrative simulation example to compare the proposed FTSM+E, which is grid-free and event-based, with two cell-based discrete-time simulation models: one based on applying a Godunov-like scheme using the Riemann problem solutions, and another using approximate expressions for the SoC dynamics. The proposed FTSM+E is shown to be able to provide very detailed solutions, practically at the level of single vehicles, whereas the cell-based simulation models provide a good approximation, at the cost of loss of information due to averaging. It is notable that the approximated CTE model achieves a comparable performance to the model where the Godunov-like scheme is applied rigorously, in spite of significantly lower numerical complexity.

The proposed models are intended to be used for electromobility control, i.e., controlling the behaviour of the EVs and the broader coupled transportation and power system, in order to achieve some control goals. While in this work no control laws

were discussed, the proposed models can be used to predict the effect of various control actions and design control laws. The more complex and exact FTSM+E can be used for detailed analysis, and also to provide a ground truth for designing model approximations, whereas the simpler approximated models are more suitable for real-time control implementation.

Apart from designing control laws, there are also many other directions this work could be extended. Notably, the on- and off-ramp flows discussed here were only defined in rather simplistic terms, as piecewise-constant in time and not depending on the local traffic state. In the FTSM+E framework, the most straightforward way of remedying this is through introducing another type of transitions, which would ensure that the traffic state and flows around on- and off-ramps follow some chosen logic, e.g., through defining splitting ratios towards off-ramps. Furthermore, although the charging station implementation of the CTEC model from [14] was not explicitly considered in this work, it is not hard to also express this part of the model in a similar front-tracking framework.

Finally, this work can be seen as the first step towards studying more general second-order macroscopic traffic models in the front-tracking framework. In particular, the well-known ARZ model has many similarities with the model studied in this work, with the crucial difference being that in the case of ARZ the advected quantity also affects the traffic dynamics, resulting in full coupling between the two states. In case of the CTE model, we were able to find exact solutions, assuming the flux functions were continuous and piecewise-linear, but this is not likely to be possible in the general case. Instead, we will need to introduce approximations and quantify how they affect the discrepancy of the model from the exact solution.

Acknowledgements

This project has received funding from the European Research Council (ERC) under the European Union's Horizon 2020 research and innovation programme (grant agreement 694209), http://scalefreeback.eu.

References

[1] G. Conway, A. Joshi, F. Leach, A. García, and P. K. Senecal, "A review of current and future powertrain technologies and trends in 2020," *Transportation Engineering*, vol. 5, p. 100 080, 2021.

[2] L. P. Fernandez, T. G. San Román, R. Cossent, C. M. Domingo, and P. Frias, "Assessment of the impact of plug-in electric vehicles on distribution networks," *IEEE transactions on power systems*, vol. 26, no. 1, pp. 206–213, 2010.

[3] M. B. Arias, M. Kim, and S. Bae, "Prediction of electric vehicle charging-power demand in realistic urban traffic networks," *Applied energy*, vol. 195, pp. 738–753, 2017.

[4] F. Mwasilu, J. J. Justo, E.-K. Kim, T. D. Do, and J.-W. Jung, "Electric vehicles and smart grid interaction: A review on vehicle to grid and renewable energy sources integration," *Renewable and sustainable energy reviews*, vol. 34, pp. 501–516, 2014.

[5] C. Le Floch, E. C. Kara, and S. Moura, "PDE modeling and control of electric vehicle fleets for ancillary services: A discrete charging case," *IEEE Transactions on Smart Grid*, vol. 9, no. 2, pp. 573–581, 2016.

[6] G. Wenzel, M. Negrete-Pincetic, D. E. Olivares, J. MacDonald, and D. S. Callaway, "Real-time charging strategies for an electric vehicle aggregator to provide ancillary services," *IEEE Transactions on Smart Grid*, vol. 9, no. 5, pp. 5141–5151, 2017.

[7] M. Alizadeh, H.-T. Wai, M. Chowdhury, A. Goldsmith, A. Scaglione, and T. Javidi, "Optimal pricing to manage electric vehicles in coupled power and transportation networks," *IEEE Transactions on control of network systems*, vol. 4, no. 4, pp. 863–875, 2016.

[8] Z. Zhou, X. Zhang, Q. Guo, and H. Sun, "Analyzing power and dynamic traffic flows in coupled power and transportation networks," *Renewable and Sustainable Energy Reviews*, vol. 135, p. 110 083, 2021.

[9] C. Fiori, K. Ahn, and H. A. Rakha, "Power-based electric vehicle energy consumption model: Model development and validation," *Applied Energy*, vol. 168, pp. 257–268, 2016.

[10] X. Qi, G. Wu, K. Boriboonsomsin, and M. J. Barth, "Data-driven decomposition analysis and estimation of link-level electric vehicle energy consumption under real-world traffic conditions," *Transportation Research Part D: Transport and Environment*, vol. 64, pp. 36–52, 2018.

[11] F. Morlock, B. Rolle, M. Bauer, and O. Sawodny, "Forecasts of electric vehicle energy consumption based on characteristic speed profiles and real-time traffic data," *IEEE Transactions on Vehicular Technology*, vol. 69, no. 2, pp. 1404–1418, 2019.

[12] B. Luin, S. Petelin, and F. Al-Mansour, "Microsimulation of electric vehicle energy consumption," *Energy*, vol. 174, pp. 24–32, 2019.

[13] M. Ross, L. Du, and B. Seibold, "Spatial-temporal ev charging demand model considering generic second-order traffic flows," in *2021 IEEE Transportation Electrification Conference & Expo (ITEC)*, IEEE, 2021, pp. 789–794.

[14] M. Čičić and C. Canudas-de-Wit, "Coupled macroscopic modelling of electric vehicle traffic and energy flows for electromobility control," in *61st IEEE Conference on Decision and Control (CDC)*, 2022.

[15] M. D. Simoni and C. G. Claudel, "A fast simulation algorithm for multiple moving bottlenecks and applications in urban freight traffic management," *Transportation Research Part B: Methodological*, vol. 104, pp. 238–255, 2017.

[16] P.-E. Mazaré, A. H. Dehwah, C. G. Claudel, and A. M. Bayen, "Analytical and grid-free solutions to the Lighthill–Whitham–Richards traffic flow model," *Transportation Research Part B: Methodological*, vol. 45, no. 10, pp. 1727–1748, 2011.

[17] S. Godunov and I. Bohachevsky, "Finite difference method for numerical computation of discontinuous solutions of the equations of fluid dynamics," *Matematičeskij sbornik*, vol. 47, no. 3, pp. 271–306, 1959.

[18] J. Glimm, E. Isaacson, D. Marchesin, and O. McBryan, "Front tracking for hyperbolic systems," *Advances in Applied Mathematics*, vol. 2, no. 1, pp. 91–119, 1981.

[19] C. F. Daganzo, "The cell transmission model: A dynamic representation of highway traffic consistent with the hydrodynamic theory," *Transportation Research Part B: Methodological*, vol. 28, no. 4, pp. 269–287, 1994.

[20] M. Čičić and K. H. Johansson, "Front-tracking transition system model for traffic state reconstruction, model learning, and control, with application to stop-and-go wave dissipation," *Transportation Research Part B: Methodological*, 2022.

[21] Adimurthi, J. Jaffré, and G. V. Gowda, "Godunov-type methods for conservation laws with a flux function discontinuous in space," *SIAM Journal on Numerical Analysis*, vol. 42, no. 1, pp. 179–208, 2004.

[22] M. L. Delle Monache and P. Goatin, "A front tracking method for a strongly coupled PDE-ODE system with moving density constraints in traffic flow," *Discrete and Continuous Dynamical Systems-Series S*, vol. 7, no. 3, pp. 435–447, 2014.

[23] M. L. Delle Monache, J. Reilly, S. Samaranayake, W. Krichene, P. Goatin, and A. M. Bayen, "A pde-ode model for a junction with ramp buffer," *SIAM Journal on Applied Mathematics*, vol. 74, no. 1, pp. 22–39, 2014.

[24] J.-P. Lebacque and M. M. Khoshyaran, "A variational formulation for higher order macroscopic traffic flow models of the gsom family," *Procedia-Social and Behavioral Sciences*, vol. 80, pp. 370–394, 2013.

[25] M. J. Lighthill and G. B. Whitham, "On kinematic waves II. a theory of traffic flow on long crowded roads," *Proceedings of the Royal Society of London. Series A. Mathematical and Physical Sciences*, vol. 229, no. 1178, pp. 317–345, 1955.

[26] P. I. Richards, "Shock waves on the highway," *Operations research*, vol. 4, no. 1, pp. 42–51, 1956.

[27] A. Aw and M. Rascle, "Resurrection of "second order" models of traffic flow," *SIAM journal on applied mathematics*, vol. 60, no. 3, pp. 916–938, 2000.

[28] H. M. Zhang, "A non-equilibrium traffic model devoid of gas-like behavior," *Transportation Research Part B: Methodological*, vol. 36, no. 3, pp. 275–290, 2002.

[29] J.-P. Lebacque, S. Mammar, and H. Haj-Salem, "The aw–rascle and zhang's model: Vacuum problems, existence and regularity of the solutions of the riemann problem," *Transportation Research Part B: Methodological*, vol. 41, no. 7, pp. 710–721, 2007.

[30] R. E. Ferreira and C. I. Kondo, "Glimm method and wave-front tracking for the aw-rascle traffic flow model," *Far East J. Math. Sci.(FJMS)*, vol. 43, no. 2, pp. 203–223, 2010.

[31] H. Holden and N. H. Risebro, *Front Tracking for Hyperbolic Conservation Laws*. Springer, 2015, vol. 152.

[32] Y. Lu, S. C. Wong, M. Zhang, and C.-W. Shu, "The entropy solutions for the Lighthill-Whitham-Richards traffic flow model with a discontinuous flow-density relationship," *Transportation Science*, vol. 43, no. 4, pp. 511–530, 2009.

[33] C.-X. Wu, P. Zhang, S. Wong, and K. Choi, "Steady-state traffic flow on a ring road with up-and down-slopes," *Physica A: Statistical Mechanics and its Applications*, vol. 403, pp. 85–93, 2014.